Remote sensing for sustainable river management: Evaluating watershed vulnerability for Ganga, the world's most densely populated river basin

Anthony Acciavatti[1,2*], Sarthak Arora[2], Michael Warner[2], Ariel Chamberlain[2], James C. Smoot[2], Nikhil Raj Deep[2,3], Claire Gorman Hanly[2,4]

1 Yale School of Architecture, 180 York St, New Haven, CT, 06511, United States
2 Collaborative Earth, 1080 Jones St, Berkeley, CA, 94710, United States
3 University of Florida IFAS Department of Soil, Water, and Ecosystem Sciences, 2181 McCarty Hall A, Gainesville, FL, 32611, United States
4 MIT School of Architecture and Planning, 77 Massachusetts Ave building 10-400, Cambridge, MA, 02139, United States

* anthony.acciavatti@yale.edu

Abstract

When standing water mixes with wastewater, it can create serious public health and environmental concerns. This scenario is particularly dangerous in densely populated urban areas with inadequate infrastructure. Such contamination threatens to cause major public health crises in the Ganga River basin where monsoonal flooding, which is exacerbated by climate change, converges with 6 billion liters of untreated sewage that is discharged daily into the river by 650 million people. To prioritize areas of the watershed for actions ranging from conservation to intervention, it is vital to perform vulnerability assessments. While the Analytic Hierarchy Process (AHP) is widely regarded as the standard in decision making methodologies, uncertainties arise from its dependence on expert judgments, especially when applied to remote sensing data, where expert knowledge might not fully capture spatial and spectral complexities inherent in such data. To constrain model uncertainties, AHP alongside a suite of alternative existing and novel variants of AHP-based decision analysis was applied on remote sensing data to assess the vulnerability of the river Ganga to pollution. Model outputs were compared to identify areas where variants may provide additional insights over AHP, and a composite variable of these results was utilized to robustly define the vulnerability of the river Ganga to waterway pollution. Together, these analyses located areas of extreme vulnerability at the nexus of river Ganga and urban landscapes as well as regions of low vulnerability potentially suitable for conservation efforts or sustainable development practices to prevent their degradation. This approach contributes to a more comprehensive understanding of remote sensing data applications in environmental assessment, and these decision-making variants can also have broader applications in other areas of environmental management and sustainability, facilitating more precise and adaptable decision support frameworks in densely populated watersheds.

Introduction

India is home to the world's largest population and most populated river basin: Ganga. While it spans across Bangladesh, Nepal, and Tibet, the majority of the Ganga basin and its population resides within present-day India. Not only is the Ganga basin densely populated, but it also remains agriculturally productive and receives significant rainfall during the southwest monsoon season (June-September); all three factors compound its vulnerability to pollution and disease vectors.

The acute and chronic impacts of human activities on the river Ganga are physical, chemical, and biological [1; 2]. For instance, the Ganga Basin is physically transformed with several barrages (i.e. dams) as well as an extensive irrigation system that diverts the Himalayan discharge away from river Ganga to support agriculture through the basin. Moreover, changes in water chemistry along the river are driven by a variety of factors, including industrial waste and synthetic fertilizer runoff, along the length of the river [3]. Additionally, Srinivas et al. [4] identified 13 threats and challenges impacting the river Ganga that included broad concerns ranging from biodiversity loss to open defecation near the river. To reduce anthropogenic induced threats and increase the overall health of the river basin, river rejuvenation and development must simultaneously address multiple social, economic, and environmental dimensions [5].

In order to prioritize areas of the Ganga basin for actions such as conservation, restoration, intervention, and rejuvenation, it is crucial to perform vulnerability assessments. There are many vulnerability assessment methods, and a multitude of factors, dimensions, and subdimensions may be included in an assessment [6]. Critically, our assessment considers not only the immediate vulnerability of a given area but also the threat to the broader river system posed by potential sources of pollution in that area. This approach properly recognizes that the interaction of pollutants with local geophysical factors creates variation in environmental impacts downstream.

The Analytical Hierarchical Process (AHP) is a multicriteria decision making process that combines pairwise comparisons and expert judgements to arrive at its conclusions. Developed by Saaty [7], AHP has been used in numerous applications, ranging from resource allocation and site prioritization to risk assessment and conflict resolution. Climate and geophysical models have proven well-suited for AHP, due to the complexity of decision making under uncertainty with respect to factors impacting their features of interest. For example, Jhariya et al. [8] used AHP in combination with Geospatial Information Systems (GIS), remote sensing, and vertical electrical soundings (VES) to identify potential zones of groundwater using weighted data on geology, geomorphology, rainfall, lineament, LULC (land use and land cover), drainage density, slope, soil type, and soil texture. Using AHP, they were able to estimate the likelihood of groundwater in each zone, with five levels of potential (low, medium, medium-high, high, and very high) with an accuracy of 80%.

AHP factors of waterway vulnerability and their Saaty rankings

In this study, AHP was used as a characterization scheme rather than a decision making process; hence, factors and their relative rank order of importance were structured to highlight areas that may be vulnerable to pollution with an emphasis on urban pollution. Land use was identified using LULC, a widely recognized direct characterization of land types and includes development such as urbanization and agricultural uses. Urbanization may be directly related to major sources of contamination in water bodies, while agriculture is a major source of nonpoint source pollution including fertilizers and pesticides. Moreover, densely populated areas have a direct impact on surface water quality. For instance, population growth rate and water quality parameters, such as biochemical oxygen demand (BOD) and dissolved oxygen, were highly correlated in a Kelani river watershed in Sri Lanka [9]. Given our emphasis on urban pollution and their direct impacts on vulnerability to pollution, population density (PD) was ranked as the most important factor (1 on the Saaty-scale), and LULC was ranked second with a Saaty-scale value of 2 in relative importance.

Rainfall, slope, and drainage density indirectly impact vulnerability in that they are not sources of pollution, yet they directly influence erodibility and pollution mobility. For example, the runoff from steeper slopes was more likely to carry pollutants into streams than runoff from land use in flatter slopes [10], and effects on water quality originating from land use (agriculture, industrial, and residential) adjacent to water bodies were dependent on rainfall variability [11]. Drainage density (DD) is an indicator of surface runoff processes and direct runoff and pollution transport increase with greater DD [12]. Rainfall, DD, and slope were assigned Saaty-scale values of 4, 5, and 7 respectively because rainfall initiates pollutant movement events, slope is an important factor in pollutant transport, and DD influences final distribution of pollutants. Temperature is an environmental determinant of microbial activity and productivity including nuisance algal blooms. For instance, water surface temperature behavior in zones with algal bloom occurrences presented greater significant values, up to 3°C, than those with clearer water [13]. Moreover, seasonal increases of anaerobic bacteria in aquatic surface sediment during summer compared to cool months indicated a depletion of oxygen in the overlying water [14]. Given the absence of high resolution site monitoring throughout the Ganga basin, land surface temperature (LST) was used as a surrogate temperature estimate. LST was assigned the lowest importance among all input factors (9 on the Saaty-scale) because it was expected to have a minor overall relative impact on vulnerability.

Potential Shortcomings of AHP

While AHP offers numerous advantages in terms of decision making in remote sensing, Munier and Hontoria [15] identified 30 potential shortcomings of the method. Given the importance of accurately understanding vulnerability, we reviewed all the shortcomings of AHP and assessed whether they were applicable for remote sensing data and our particular use case (S1 Table). For instance, the first critique "The Pair-Wise Method and Its Application in AHP" suggested that some problems may not be suited for AHP if their decision space is amorphous with many interrelated factors that have minimal differences in their relative importance. This critique was not applicable for our use-case, since our problem fits well to the AHP architecture. Similarly, the critique around rank reversals, which arise when uncertainty in the decision space is larger than the consistency of rank, was applicable on our use-case since a change in parameter weights might lead to an inaccurate assessment of the vulnerability of the river. To test for this and design a better method, we applied AHP while taking into account the effect of unknown variables (1-N AHP) and Fuzzy AHP as diagnostic analyses. To summarize, all the applicable shortcomings were addressed with the following approaches: Analytic Network Process (ANP) [16], Fuzzy AHP [17] , AHP with non-linear parametric influence (Nested AHP), 1-N AHP, and Fuzzy AHP while taking into account the effect of unknown factors (Fuzzy 1-N AHP) (S1 Table).

In this paper, we apply AHP to our remote sensing datasets to assess the vulnerability of the river Ganga to pollution loads along a 1,330 km stretch of the river. We cover the problem formulation, results and inferences of AHP. We also include a deep-dive on each shortcoming of AHP in the context of Climate Modelling, addressing the list set forth by Munier and Hontoria [15]. We share whether each shortcoming was applicable to our problem statement, while suggesting and attempting alternative solutions to counteract the shortcomings. Through this dialogical process, we have arrived at two novel decision making approaches inspired by AHP, namely Nested AHP and 1-N AHP. The methodological contributions of this research are, at one level, these new variants of AHP we propose; and at another level, the demonstration of how incremental evaluation of the AHP process and its shortcomings relative to a given problem can reveal application-specific permutations of the original. Finally, we report the pollution vulnerability evaluation of the river Ganga produced by these processes.

Methods and Data

Study area and data source

The area of analysis (26,609.4 km^2) is a 20 km zone extending 10 km on both sides of the main channel of river Ganga from Haridwar, Uttarakhand, where it makes its debouche from the Siwalik Hills into the Indo-Gangetic plains to its confluence with river Ghaghara at Sitab Diara, Uttar Pradesh, India (Fig 1).

Fig 1. Ganga Inset Map This map shows the Ganga Basin, in gray, and the buffer region, in blue, which is the scope of our paper. The 20 km buffer zone extends 10 km on both sides of the main channel of river Ganga.

The change in elevation along this 1,330 km stretch of Ganga is from 314 m to 76 m above mean sea level. Data from Landsat-8 (Level 2, Collection 2, Tier 1; pixel resolution, 30x30m) and other sources (S2 Table) were used to assess vulnerability in the area of analysis include slope, drainage density (DD), land surface temperature (LST), rainfall, land use/land cover (LULC), and population density (Fig 2). The drainage density and center line for the river Ganga were both derived from a digital elevation model (DEM) of the watershed using typical GIS hydrography processes, as previously described by Rahaman et al. [18]. Streams were extracted from NASADEM data as a vector format Shapefile using the R programming language, Whitebox, Terra, and sf packages. Lower order streams were removed to obtain the main Ganga river centerline with ArcGIS Pro. The Ganga center line down-river of the Uttar Pradesh border was removed, and the 20 km zone was established as a buffer around this shortened centerline within the river Ganga.

Fig 2. AHP Factor Layers Visual representation of the data used in the calculation of AHP. AHP factors Population Density (a), Annual Rainfall (c), Drainage Density (d), Slope (e), and Land Surface Temperature (LST) (f) were divided into extreme low to extreme high using natural breaks. AHP factor Land Use Land Cover (LULC) (b) was separated by land use class. Factor classes were based on natural breaks. Factor classification indicates how much impact each variable has on vulnerability.

Analytical Hierarchy Process (AHP)

To categorize the vulnerability of the area immediately around the river Ganga and to identify potential locations to implement our remediation strategies, we applied the AHP on Remote Sensing and other geospatial data as previously described by Jhariya et al. [8]. Environmental, topographical, and anthropogenic factors were ranked from equal importance to relatively greatest hierarchical importance across the full breadth of the 9-point Saaty scale based on their likelihood of impacting vulnerability. A pairwise matrix constructed from these ranked factors and their reciprocal values were used to estimate a mean normalized weight for each factor (S3 Table). These normalized weights were applied to each of five factor classes that were identified by natural breaks in the data using the Jenks method. LULC categories were numerically scored as vulnerability criteria based on their linkage to pollution. Lastly, overall vulnerability per pixel was determined from the sum of the factor vulnerability scores. Additional details describing factor rank orders, pairwise comparison matrices and their weights, as well as Jenks natural breaks are provided in Supporting Information (S1 Text and S2 Text).

If:

- W is the 1x6 row vector of AHP weights:

$$W = \begin{bmatrix} w_1 & w_2 & w_3 & w_4 & w_5 & w_6 \end{bmatrix} \quad (1)$$

- $X(p)$ is the 1x6 row vector of parameter values at pixel p for the six factors:

$$X(p) = \begin{bmatrix} x_1(p) & x_2(p) & x_3(p) & x_4(p) & x_5(p) & x_6(p) \end{bmatrix} \quad (2)$$

We calculated the predicted vulnerability for each pixel by multiplying each factor's parameter value by its corresponding AHP weight i.e. the dot product of the vector W with the transpose of the vector $X(p)$:

$$V(p) = W \cdot X(p)^T \quad (3)$$

Eq (1), (2) and (3) were used to create the vulnerability map of the Ganga buffer region. We used Google Earth Engine to multiply the AHP weights with the bucketed values for each layer at each pixel and aggregated them to get our final vulnerability scores for the entire Ganga buffer. More information about the Remote Sensing datasets we used on Google Earth Engine can be found in S2 Table.

Diagnostic Analyses

Nested AHP

We performed the AHP analysis under the assumption that while each parameter contributes to the vulnerability differently, the contribution of each parameter to vulnerability was linear in nature i.e. areas where the value of a parameter was 5 contributed to the vulnerability 5 times more than areas where the value was 1. This is an overly simplified approach; hence, we created a pairwise matrix for each factor, using the bucketed values for the parameters, and performed AHP on each parameter with itself, to create the Nested AHP approach (S3 Text).

Fuzzy AHP

Fuzzy Analytic Hierarchy Process (Fuzzy AHP), as introduced by Saaty [17] is an extension of the classic AHP that incorporates the fuzziness (probabilistic alterations/error) associated with human judgment. By using fuzzy numbers in the rankings, Fuzzy AHP accommodates these uncertainties and thus provides more reliable results.

To understand the robustness of our AHP factor rank order results, we utilized fuzzy AHP to see if there was an inconsistency within the results, i.e. if there was a rank reversal between the parameters when we incorporate fuzziness to the values of the AHP pairwise comparison matrix (S4 Text).

ANP

One of the main limitations of AHP is its inability to adequately capture the interdependencies among criteria and alternatives. To address this issue, Saaty [16] developed ANP, which extends the AHP methodology by accommodating feedback loops and interdependencies among criteria and alternatives. Unlike AHP, which assumes a hierarchical structure, ANP allows for the representation of complex relationships and feedback loops in decision networks. The method utilizes a supermatrix to integrate both local and global influences, providing a more realistic representation of environments. ANP is widely used to represent interdependent relationships, making it suitable for decision problems with interconnected elements. ANP introduces the concept of contextual weights, enabling decision makers to adjust the importance of criteria and alternatives based on the context of the decision problem. This flexibility enhances the adaptability of ANP to various situations.

In a complex system such as the geophysical environment, it is expected that AHP factors will be correlated to one another. While AHP assumes strict independence between criteria at different levels of the hierarchy, ANP allows for both dependence and independence relationships (Table 1) as described previously by Poh and Liang [20]; this flexibility better captures the intricacies of decision networks across natural systems.

Table 1. Vulnerability ANP Supermatrix[a]

	Goal	**Criteria**	**Subcriteria**	**Alternative outcomes**
Goal	0	0	0	0
Criteria (AHP factors)	W21	W22	0	0
Subcriteria (vulnerability classes)	0	W32	W33	0
Alternative outcomes	0	0	W34	I

[a] ANP Criteria were AHP factors, and ANP Subcriteria were AHP vulnerability rankings.
The ANP supermatrix component matrices as follows:

- Relative importance of criteria (AHP factors), W_{21};
- Inner dependence (As defined by [20]) matrix of criteria, W_{22};
- Relative importance of subcriteria (vulnerability classes) w.r.t criteria, W_{32};
- Inner dependence matrix of subcriteria, W_{33};
- and Relative importance of subcriteria w.r.t alternatives, W_{34}.

$$W_{21} = \begin{bmatrix} 0.408 \\ 0.268 \\ 0.138 \\ 0.1 \\ 0.058 \\ 0.028 \end{bmatrix} \qquad W_{22} = \begin{bmatrix} 0.464 & 0.233 & 0.14 & 0.277 & 0 & 0.186 \\ 0.271 & 0.408 & 0.12 & 0.098 & 0 & 0.077 \\ 0.105 & 0.126 & 0.662 & 0 & 0 & 0 \\ 0.085 & 0.079 & 0 & 0.498 & 0 & 0 \\ 0.076 & 0.079 & 0.078 & 0.126 & 0 & 0 \\ 0 & 0.075 & 0 & 0 & 0 & 0.737 \end{bmatrix}$$

$$W_{32} = \begin{bmatrix} 0.572 & 0.505 & 0.501 & 0.642 & 0.388 & 0.557 \\ 0.207 & 0.186 & 0.172 & 0.157 & 0.233 & 0.165 \\ 0.114 & 0.144 & 0.124 & 0.071 & 0.276 & 0.129 \\ 0.057 & 0.11 & 0.102 & 0.065 & 0.07 & 0.099 \\ 0.05 & 0.055 & 0.102 & 0.065 & 0.033 & 0.05 \end{bmatrix} \qquad W_{33} = O_{5x5}$$

$$W_{34} = \begin{bmatrix} 0.56 & 0.61 & 0.571 & 0.483 & 0.409 \\ 0.187 & 0.203 & 0.229 & 0.276 & 0.273 \\ 0.112 & 0.102 & 0.114 & 0.138 & 0.182 \\ 0.08 & 0.051 & 0.057 & 0.069 & 0.091 \\ 0.062 & 0.034 & 0.029 & 0.034 & 0.045 \end{bmatrix} \qquad I = I_{5x5}$$

The calculation of each component matrix is available in the "ANP supermatrix and inner dependence pairwise comparisons" section in the Supplemental Information (S5 Text).

We generated the ANP supermatrix with the goal to assign pollution vulnerability scores (PVS). Here the AHP Factors, or Criteria were - Population density, LULC, rainfall, drainage density, slope and temperature. The Alternatives were pertaining to the PVS, i.e., extremely high, high, moderate, low, extremely low. The possible relationship arcs were dependencies, self-loops, and feedbacks.

We used the Python library pyanp created by Adams et al [21] to run the ANP Algorithm on the Supermatrix.

1-N AHP

Another shortcoming of AHP is that, from inside the process, there is no way of knowing for certain if there are any important factors missing from the decision problem parameters. For AHP, our model was considering six factors - Population density, LULC, rainfall, drainage density, slope and temperature. If a fundamental pollution vulnerability factor was missing, AHP would not capture it.

To overcome this, we devised an approach named 1-N AHP where we aimed to validate whether the unknown and unconsidered factors are important for our analysis of vulnerability or not (S6 Text).

Fuzzy 1-N AHP

We have described two approaches to deal with the complex nature of decision making methods for environmental problems. While Fuzzy AHP took into account the potential error in the decision maker's choice for the values of the pairwise comparison matrix, 1-N AHP considered unknown factors which we may have missed while considering the vulnerability of a river. Since both approaches were mutually exclusive, we performed one final test to check the robustness of our results by combining these two approaches.

We performed 1-N AHP followed by a fuzzy analysis on the values. First, we used our eight weights (six original weights, plus a weight each for aggregated acute and chronic factors) that we derived from our analysis in 1-N AHP, and applied linear algebra to create our new matrix (i.e. because the AHP vector output is the eigenvector, and the eigenvalue is used to calculate the confidence, we used $A = PDP^{-1}$ to get back our original matrix A, where P is a matrix of eigenvectors and D is a diagonal matrix of eigenvalues). We then ran Fuzzy AHP on this new 8x8x3 matrix for 100,000 simulations to get the 8x1 size priority vectors. From these vectors, we randomly excluded the acute factors for 97.5% of the cases, and in 75% of the 100,000 cases, the chronic factors were randomly excluded, before checking the rank reversals. This was to account for the probabilities of the presence (or absence) of acute and chronic factors respectively while checking for rank reversals.

Results

River Ganga vulnerability based on AHP

Given our pairwise matrix, we obtained the importance weights of parameters as 0.408, 0.268, 0.138, 0.100, 0.058, 0.028 for Population Density (PD), LULC, Rainfall (RAIN), Drainage Density (DD), Slope, Land Surface Temperature (LST) respectively. We multiplied the pixel values for each parameter with their weights to get our final output layer, which represented the vulnerability map of the River Ganga (Fig 3).

AHP vulnerability scores ranged from a minimum of 1.001 to a maximum of 4.470 with 83.7% of the area being categorized as having extremely low or low vulnerability and 3.5% of the area is highly or extremely high vulnerability (Fig 3(b)). Tier 2 cities (i.e., cities with a population between 50,000 and 99,999 people) on the banks of river Ganga such as Varanasi, Prayagraj/Allahabad, and Kanpur were clearly highlighted with high and extremely high AHP vulnerability scores (Fig 3(a)). Indeed, urban settings that had population densities $\geq$ 1,100 people km^2 typically had vulnerability scores $\geq$ 2.736. Alternatively, the areas with vulnerability scores $\leq$ 1.694 were

Fig 3. AHP, Nested AHP, ANP, and Comparison: Ganga Vulnerability Map & Histogram These figures show the vulnerability scores for AHP (a-b), Nested AHP (c-d) and ANP (e-f) for the scope of our analysis; the lower values pertained to the least vulnerable areas while the ones with higher scores were the most vulnerable. Map of exact values per pixel location (a,c,e) and histogram of binned ranges of values (b,d,f). The graph in (g) shows the normalized amount each factor class 1, 2, 3, 4, 5 affects the overall weighted overlay for AHP, Nested AHP and ANP, where blue (circles) represents AHP, red (squares) represents Nested AHP and green (triangles) represents ANP.

characterized by forest or cropland regions with low human population densities. The annual rainfall in the high elevation regions of the river Ganga generally increased the vulnerability of those regions.

Nested AHP and ANP

We used Google Earth Engine to multiply the subweights based on the bucketed value for each factor, and multiplied it with our original AHP weights to get our final vulnerability scores for the entire Ganga buffer. The new weights for the six criteria were 0.44264, 0.21335, 0.14490, 0.10835, 0.09076 for each factor class 1, 2, 3, 4, 5.

The distribution of vulnerability scores produced with both Nested AHP and ANP were markedly different from the distribution produced with AHP (Fig 3(c-f)). Specifically, Nested AHP resulted in 96.7% of the area scored as extremely low and low vulnerability, which was skewed with a right-tail range that extended 1.8-fold further than AHP. Similarly, ANP exhibited a right-tailed distribution with low vulnerability scores. Despite that, the Tier 2 cities had high vulnerability scores for both ANP and Nested AHP, except for Kanpur, which saw a major reduction in the vulnerability scores. These differences were due to the nonlinear response of factor weights to vulnerability rankings in both methods (Fig 3(g)). Thus, these methods resulted in overall focused, yet dampened, vulnerability-score maps compared to AHP. Despite the additional insights these analyses revealed, the fundamental issue of the extent to which the defined AHP factors adequately encompass the vulnerability space remained.

For ANP, the initial values of the "relative importance of subcriteria with respect to criteria (W32)" submatrix were collected from the Nested AHP analysis. To test whether the nonlinearity of this submatrix significantly affected the ANP results, we changed the matrix values from Nested AHP to original AHP. There were only minor changes from the initial ANP results (S4 Fig), suggesting that the nonlinear results of ANP were independent of the submatrix values.

1-N AHP

When we ran 1-N AHP for the worst case, N = 0.33, we attributed more weightage to the unknown acute and chronic factors than for the average case, N = 0.165. However, due to the low probability of the presence of an acute or chronic factor, the vulnerability scores were lower for the worst case than the average case (Fig 4). Even when we considered the distribution of the result values, we saw that the results for the worst case were more right skewed than the average case, which was more right skewed than the original AHP. From this we can gather that given our assumptions, there was no negative impact of considering unknown factors in our AHP analysis. However, 1-N would positively be able to capture the robustness of AHP results in other contexts, or if the assumptions were altered, and since our acute and chronic layers were purely random across the Ganga buffer, the change in vulnerability values were correlated to the values of the initial AHP results, and not to any specific remote sensing or other GIS data layers in the analysis.

Fig 4. 1 - N AHP Worst case (N = 0.33) and Average case (N = 0.165): Ganga Vulnerability Map & Histogram These figures show the vulnerability scores for 1-N AHP when we consider the worst case (N=0.33) (a-b) and average case (N=0.165) (c-d); the lower values pertained to the least vulnerable areas while the ones with higher scores were the most vulnerable. Map of exact values per pixel location (a,c) and histogram of binned ranges of values (b,d).

Fuzzy AHP and Fuzzy 1-N AHP

Out of 100,000 Fuzzy AHP simulations, there were 4,433 rank reversals and no simulation had any second-order rank reversal (cases with greater than 1 index being flipped e.g. Population Density and Rainfall) at 95% fuzziness. This implied that there was a 4.43% chance of rank reversals at 95% fuzziness. Of these reversals, the vast majority occurred between the factors Rainfall and Drainage Density (Table 2), which can be attributed to the low percentage difference between their initial values.

Table 2. Count of Rank Reversals for Fuzzy AHP out of 100,000 simulations

Reversals between Parameters[a]	Range of Original AHP results	Count of Rank Reversals
PD and LULC	(0.408, 0.268)	45
LULC and Rainfall	(0.268, 0.138)	30
Rainfall and DD	(0.138, 0.1)	4233
DD and Slope	(0.1, 0.058)	146
Slope and LST	(0.058, 0.028)	49

[a]Here, PD is Population Density, LULC is Land Use Land Cover, DD is drainage density, and LST is Land Surface Temperature

The simulations with rank reversals were tested to determine their potential impact on vulnerability scores. This was done by running AHP on a sample of 500 from the 4,433 cases where a rank reversal occurred, and averaging all the output layers to return the Mean Fuzzy AHP layer (Fig 5(a-b)). Of these, areas that experienced changes in vulnerability due to rank reversals had high Drainage Density, or were areas that tended to receive large amounts of precipitation.

Fig 5. Fuzzy AHP Mean, Case 1 and Case 2: Ganga Vulnerability Map & Histogram These figures show the vulnerability scores for Fuzzy AHP's Mean case (a-b), Case 1 (c-d) and Case 2 (e-f) for the scope of our analysis; the lower values pertained to the least vulnerable areas while the ones with higher scores were the most vulnerable. Map of exact values per pixel location (a,c,e) and histogram of binned ranges of values (b,d,f).

We also tested the change in vulnerability for two cases with the biggest rank reversal (i.e., the worst case). There can be two ways with the biggest rank reversals:

- **Case 1:** When there was a rank reversal between the two factors that have the highest weightage (i.e., Population Density and LULC, with the highest delta between the weights).
- **Case 2:** When the difference between the fuzzy AHP results for a simulation had the highest delta with the values of the original AHP factor weights.

For both the cases (Fig 5(c-f)), we saw the distribution skewed to the left as compared to the original AHP, and the vulnerability increased, which was more prominent for Case 2 (Fig 5(e-f)). Due to the high weightage of the parameter, there was a increase in vulnerability scores in the areas with high population density.

For Fuzzy 1-N AHP, there were 15,413 rank reversals out of 100,000 AHP simulations, suggesting a 15.4% chance of rank reversals (Table 3). There were around 200 second-order rank reversals as well (Table 4). Most of the rank reversals were between the factors Slope and Chronic, followed by Rainfall and DD, similar to Fuzzy AHP. A major contributor to the rank reversals was the closeness of the original AHP weights, leading to a higher likelihood of rank reversals when fuzziness is incorporated.

Table 3. Count of First-order Rank Reversals for Fuzzy 1-N AHP out of 100,000 simulations

Reversals between Parameters	Range of Original AHP results	Count of Rank Reversals
Acute and PD	(0.297, 0.27336)	185
PD and LULC	(0.27336, 0.17956)	854
LULC and Rainfall	(0.17956, 0.09246)	21
Rainfall and DD	(0.09246, 0.067)	6054
DD and Slope	(0.067, 0.03886)	966
Slope and Chronic	(0.03886, 0.033)	7220
Chronic and LST	(0.033, 0.01876)	447

Table 4. Count of Second-order Rank Reversals for Fuzzy 1-N AHP out of 100,000 simulations

Reversals between Parameters	Range of Original AHP results	Count of Rank Reversals
Acute and LULC	(0.297, 0.17956)	0
PD and Rainfall	(0.27336, 0.09246)	0
LULC and DD	(0.17956, 0.067)	0
Rainfall and Slope	(0.09246, 0.03886)	5
DD and Chronic	(0.067, 0.033)	77
Slope and LST	(0.03886, 0.01876)	117

Comparison of analysis scores

To compare different approaches and test areas where the predicted vulnerability changes, we normalized the different output layers by standardizing them to follow Normal distributions with a Mean of 0 and Standard Deviation of 1, i.e. Standard Normal Distribution. This enabled us to compare different approaches that had different ranges. Then we subtracted each output layer from the original AHP results, i.e. AHP Vulnerability Score - Variant Vulnerability Score, to get our final distribution of difference layers. While computing these layers, the positive values showed that as per AHP, the areas were identified as more vulnerable than the variant map did, and the vice versa in case of negative values.

We compared the results of every other approach with the original AHP results, using AHP as the baseline for checking the robustness of our approaches. We wanted to infer three things from the distribution of difference layers, 1) Which pixel values changed relative to AHP, 2) How much did they change, 3) Were the changed values higher or lower than AHP?

Also, since the effect of Population Density on vulnerability was high, we conducted the same difference test to assess whether the Population Density layer by itself could suffice in assessing the vulnerability of the basin. This tells us how much of the variability of the vulnerability score can be attributed solely to Population Density.

To visualize and compare the distributions of differences of the AHP layer with other approaches, we created 3 different map types (S5 Fig). We created Map Type 1 by stretching the colors between the overall min max of all the different approaches, to compare the approaches among themselves. For Map Type 2 we stretched the colors between the local minimum and maximum value of each approach, to make outliers and all instances with high variability ($\geq$ 2 standard deviations (SD)) for each individual map stand out. And for Map Type 3, we stretched the colors between the local 5 percentile and 95 percentile for each approach, to prevent the values $\geq$ 2SD from washing-out the differences in the map.

Difference between Nested AHP, ANP and AHP

Observing Nested AHP and ANP, we saw a similar pattern of differences with AHP, owing to the non-linear distribution of both the results. While the AHP predicted the vulnerability to be high in Kanpur, ANP and Nested AHP suggest that it would be lower. And the vice versa is seen to be true for Prayagraj/Allahabad and Varanasi, where AHP predicted the vulnerability to be lower than the results of ANP and Nested AHP.

Difference between 1-N AHP and AHP

Despite the different visualization approaches, there were no major differences for the vulnerability scores of 1-N AHP with AHP. This can be explained by the probabilistic layers of acute and chronic error, and the fact that the factors other than acute and chronic are strongly correlated with the AHP variables.

Difference between Fuzzy AHP cases (Mean, Case 1, and Case 2) and AHP

In the Mean Fuzzy AHP Case, we sampled some of the simulations, and most of them had a rank reversal between rainfall and drainage density, causing those layers to reduce the robustness of the results. In Case 1 and Case 2, both approaches were in agreement with each other across the latter half of the Ganga buffer, but we see that in the high-altitude areas they were tending in opposite directions. In Case 1 the AHP suggested a higher vulnerability than Fuzzy AHP, primarily affected by Population Density, and in Case 2, Fuzzy AHP returned a higher value for vulnerability scores, owing to the Annual Rainfall variable.

Difference between Population density and AHP

The differences between the standardized values of AHP and the Population density layers were the highest among all approaches, and there were many areas where there is a non-zero value for this layer. This indicates that AHP is amply influenced by the other parameters and proves the effectiveness of the AHP approaches for creating a good composite variable.

Analysis of Variances

To compare the predictions for multiple variants at once, we calculated the standard deviation between three approaches: AHP, ANP, Nested AHP for each pixel and visualized them for our region of interest (Fig 6(a)). We noticed that the deviations were high for the tier-two cities Prayagraj/Allahabad and Varanasi. Varanasi had the highest vulnerability in terms of AHP, but the other variants of AHP brought more emphasis to Prayagraj/Allahabad as well. There were also some high deviations in the high-altitude regions near Rishikesh - a high-population city in Uttarakhand, suggesting disagreements between the approaches.

Fig 6. Standard Deviation of Normalized and Composite Layers Standard deviations of Normalized layers (a) for the approaches AHP, ANP, Nested AHP, where darker values suggest lower standard deviation, and the lighter values suggest high-standard deviations. The composite layer (b) that can be used to describe the vulnerability of the river Ganga. We assign different colors for pixels representing $\geq$ 2SD of each variant, and to showcase the positive and negative instances, we split them into two charts (c) and (d).

Composite Layer for all Approaches

To create a composite layer to capture the effect of each variant of AHP across the river buffer, we took a normalized base layer for AHP, and overlaid the outliers ($\geq$ 2SD) for each of the difference layers for Mean Fuzzy AHP, Nested AHP, and ANP (Fig 6(b-d)). To understand the distribution of the AHP base layer, and the distribution of the difference layers for Mean Fuzzy AHP, Nested AHP, and ANP, we also created the histograms of each layer (Fig 7). In the composite layer, the primary colors (red, blue, yellow) were used to depict the outliers for the individual layers, and secondary colors (orange, green, purple) were used when the effects of two AHP variants were combined. Given that the outliers could be both positive and negative, we also created separate maps for the two. These composite layers can be used as a way to depict a single variable for river Ganga's vulnerability with the effect of all AHP variants. Through these composite layers, we are illustrating the effect of AHP relative to the unique effects of the variants wherever they disagree with AHP.

We also selected four important subsections of the river buffer where the composite variable was effective in capturing the effects of each AHP variation (Mean Fuzzy AHP, Nested AHP, and ANP). There were some small areas near the river body which had high variability between AHP and all three AHP variants. We can see the effect of the combination of two variants in Fig 8 subsection C, where there were a lot of variability for both Nested AHP + ANP (violet) and Nested AHP + Mean Fuzzy AHP (green) variants.

Fig 7. Normalized AHP & its Difference with Normalized AHP Variants Here, (a) shows the Normalized AHP layer with its standard deviation, while the rest of the figures show the distribution of the differences between Normalized AHP and its corresponding AHP Variants: ANP, Mean Fuzzy AHP, and Nested AHP. (b) is Normalized AHP minus Normalized ANP. (c) is Normalized AHP minus Normalized Mean Fuzzy AHP. (d) is Normalized AHP minus Normalized Nested AHP.

Fig 8. Focused Composite Layers Subsection analysis of the composite variable for four subsections A, B, C, D, with different panels numbered 1 (all instances of $\geq$ 2SD), 2 (positive instances), and 3 (negative instances). To cover a range of distributions, we considered two rural (A, D), and two urban (B, C) subsections. Out of these, Subsection B has the city Kanpur in them, while subsection C is near Prayagraj/Allahabad and Varanasi, highly populated areas along the Ganga.

Discussion

In this paper, we aimed to assess the pollution vulnerability levels of the river Ganga using remote sensing datasets. We lacked ground truth data for pollution, making supervised learning algorithms unfeasible, and making it difficult to validate the metric. Gaining confidence around our results was critical, as decisions regarding the river's ecological health depend on a reliable assessment of vulnerability levels. In order to generate a spatial numeric dataset reflecting the pollution vulnerability of the river Ganga, we utilized the widely used AHP decision making method.

Despite the advantages of AHP, it has multiple shortcomings - one being its reliance on expert opinion which might be biased. So we explored existing alternative methods, such as ANP and Fuzzy AHP, and we designed novel variants of AHP, such as Nested AHP, 1-N AHP, and a hybrid Fuzzy 1-N AHP. Each of these approaches offered unique advantages over the original AHP approach, and contributed towards the robustness of our analysis by addressing different shortcomings of the AHP method.

For instance, AHP functions under the assumption that the criteria are independent of each other (5.2.8), which is fairly uncommon to achieve in real world scenarios, especially in ecological settings. For this reason, we used ANP to capture the criteria dependencies, and the results of ANP were accommodated into our proposed solution. Another shortcoming being addressed by our approach is that we tested the uncertainty in the decision space (5.2.24) by checking the likelihood of rank reversals using Fuzzy AHP and Fuzzy 1-N AHP, thus ensuring that our solution is robust to uncertainties in the decision space. Within Fuzzy AHP, we introduced another novel methodology which involved using Monte Carlo simulations to get randomized values of fuzziness instead of relying on the domain experts. This way we managed to quickly run a variety of scenarios of AHP while excluding the need of domain experts. Lastly, the "external" influence on decision (5.2.26) is accommodated by expanding to the breadth of all possible factors that might influence the decision space using 1-N AHP.

To conclude, we incorporated the variability of these different approaches into a new robust composite variable, one which overcomes the shortcomings of AHP. We can use this ensemble variable as an adaptable and reliable decision making tool to plan remediation methods for the river Ganga.

Although this study addressed many of AHP's known shortcomings, there were some limitations that were not addressed. Of note, the need for multiple technical experts to address the broad range of factors when assigning Saaty rankings is a valid concern. While we are an interdisciplinary group, we are not subject matter experts across all of the fields represented by the AHP input factors. To address this issue, an overall quality metric of the Saaty rankings may mitigate this issue based on the level of expertise and available data (e.g., a quality metric might consist of four levels, ranging from novice opinion to the consensus of subject matter experts). Furthermore, lack of certainty about the importance of alternative criteria and biases during ranking may be addressed by running different scenarios, as long as the decision space is fundamentally partitioned based on an overarching difference due to a given circumstance, and robust data and guidance is provided when rankings are calculated. In addition, vulnerability scores were dependent on remote sensing data resolution (e.g., population density is reported at 1 km^2 scale) and were context sensitive such that decision spaces may vary depending on the influence, conditions, and/or regulatory as well as technical mitigation potential in different biomes, nations, and jurisdictions to alleviate sources of vulnerability. Finally, dependencies and correlations between or among factors may not be well understood. While this is true, the process is iterative such that the models can be refined as additional data are gathered, factor interactions are clarified, and scenarios are tested.

Additional data layers such as GIS-based applications that track impacts may be integrated into the data process to support and hone vulnerability assessments and thus

AHP factor weights as well as improve output resolution and validation. For instance, acute factors may be known unknowns (e.g., mining locations) and unknown/ill defined unknowns (e.g., location and breadth of endangered species habitat). Similarly, potential widespread impacts such as loss of biodiversity and fragmentation of biodiversity richness are chronic factors that were excluded from our AHP vulnerability decision space but may be included in future efforts. Indeed, the approach of sand mining and waste disposal tracked by Bayazidy et al. [22] may be used to identify specific instances of these and other acute factors that require precise and timely identification. In addition, coupling biodiversity and the conservation imperative analysis of Dinerstein et al. [23] with our vulnerability assessment can further prioritize areas for conservation that were scored as low biodiversity and extremely low vulnerability. Moreover, emerging factors may be added as data are collected and the breadth and depth of the decision space grow. For instance, the environmental spread of antibiotic resistance in freshwater is tracked with molecular genetic techniques [24; 25], and coupling these data with their spatial locations can add antibiotic resistance as a vulnerability factor. Finally, high-resolution data from UAV such as that produced by Tripathi et al. [26] during their effort to combine remote sensing with drone data while cataloging riparian vegetation along the Ganga can augment and further refine LULC information to better refine vulnerability scores.

Ultimately, networks of models may be brought together to enrich landscape digital twins for design, decision making, and monitoring of real world features of landscapes. These twins become digital representations of natural and built features in landscapes. For river systems, digital twins may consist of riverscapes, the concept that integrates longitudinal characteristics of rivers with their land features [27]. Indeed, the basis for such twins already exists in regions prone to flooding. For instance, Nested AHP was used to predict five categories of flood susceptibility with nine factors based on remote sensing data in addition to soil texture, geomorphology, and geology [28]. Furthermore, AHP with nesting of four factors (land use, percent green space, per capita sewer length, and slope) was used to produce a flood vulnerability index in a section of Hanoi, Vietnam [29], and a flood susceptibility map for all of Hanoi was made with a 9-factor AHP that was ranked by subject matter experts [30]. AHP models that include cultural, socioeconomic and environmental criteria provide for wider assessments of the human condition. Recently, 20 factors representing these criteria as well as security and service functions were placed in a hierarchical structure and assessed through a survey of subject matter experts to realize a quality of life score [31]. Of note, they detected the inverse of our vulnerability scores in that quality of life tended to decrease away from city centers and the services they provide whereas cities consistently were sources of high vulnerability to the river Ganga. Thus, the perspective of the modeling scenario must be understood and integrated into the larger decision space of balance between human endeavors and nature. A richness of alternative perspectives can drive sustainable development so that factors that improve quality of life can be implemented with policies that recognize and mitigate their accompanying sources of vulnerabilities.

Conclusion

In this study, we assessed the vulnerability of the river Ganga to pollution along a 20 km wide corridor covering 26,609.4 km^2 of riverscape. We used AHP to perform a dimensionality reduction of six remote sensing datasets to create a single variable for river vulnerability. To mitigate structural limitations to AHP, our approach brought together a suite of methods and produced a set of comparative metrics to identify and refine vulnerability scores. Of note, urban landscape features with extremely high vulnerability scores and those at the interface with vulnerable areas were identified.

These findings provide the basis to rational prioritization of pollution mitigation and a list of locations for future rejuvenation. Moreover, sites currently with low vulnerability scores may be targeted for conservation or sustainable development practices to prevent their degradation. Our vulnerability score, together with other metrics such as a quality of life score [31], can enrich digital twins beyond simplistic animations and reveal their underlying environmental, social, and economic characteristics.

Supporting information

S1 Table. Shortcomings of AHP analysis rubric.

S2 Table. Data Sources

S3 Table. AHP Pairwise and Normalized Comparison Matrix

S1 Text AHP Ranking method and pairwise comparisons

We used the factors Population Density (PD), Land Use Land Cover (LULC), Rainfall (RAIN), drainage density (DD), Slope, and Land Surface Temperature (LST) to define the hierarchy order among parameters on the basis of their importance or relevance in terms of assessing pollution vulnerability. We classified the values for each parameter for each pixel within our area of interest between 1-5 to arrive at the "Factor Class" for that parameter, and we multiplied each Factor Class with the weight indicating the importance of that parameter. We computed the sum of all weighted parameters to produce the overall vulnerability of each pixel. We compared this with the classification parameter ranges as defined using AHP.

The importance of factors influencing naala vulnerability were placed in the following order: Population Density (PD) > LULC > Rainfall (RAIN) > Drainage Density (DD) > Slope > LST, and the factor importance rankings were inputs into an AHP pairwise comparison matrix (S3 Table).

S3 Table contains the pairwise comparison matrix and the Normalized AHP pairwise comparison matrix. The Principal Eigenvalue is the mean of the eigenvectors, and n is the number of factors - six.

To begin the AHP process, we constructed a pairwise comparison matrix (A), where each element a_{ij} represented the importance of criterion i relative to criterion j.

Once we created our pairwise comparison matrix, we normalized the matrix by dividing each element of a column by the sum of the elements of that column. This resulted in the normalized matrix $\tilde{A}$. The normalized matrix for our example was computed by:

$$\tilde{a}_{ij} = \frac{a_{ij}}{\sum_{i=1}^{n} a_{ij}} \tag{4}$$

The priority vector W (the eigenvector) was then derived by averaging the rows of the normalized matrix:

$$w_i = \frac{1}{n} \sum_{j=1}^{n} \tilde{a}_{ij} \tag{5}$$

This priority vector defines the AHP weights for each factor, and thus the impact of each factor on the vulnerability of Ganga.

In some situations, AHP importance rankings may produce inconsistent outcomes due to matrix properties. The Consistency Index (CI) and Consistency Ratio (CR)

were developed to test for inconsistency with a Consistency Ratio < 0.1 indicating the rankings were consistent [7]:

$$CI = \frac{\lambda_{max} - n}{n - 1} \tag{6}$$

where λ_{max} was the largest eigenvalue of the matrix A. The CR was the ratio of the CI to the Random Consistency Index (RI) for the corresponding matrix size (n):

$$CR = CI/RI \tag{7}$$

In our case, with a consistency ratio (CR) of 0.06, the matrix was considered consistent (as $CR < 0.1$). This consistency indicated that our pairwise comparison matrix was reliable for determining the weights.

S2 Text Natural breaks and AHP factor classes Data for each AHP factor were divided into five vulnerability classes using the Jenks natural breaks method [19]. The Jenks method is widely used within GIS packages to generate variance-minimization classification. Breaks were typically uneven, and were selected to separate values where large changes in value occur. For this, we used the boxplots (S1 Fig) and histograms (S2 Fig) for the layers to identify the natural breaks for each factor.

S1 Fig. AHP Box and Whisker Plot Summary Panels (a) through (e) are box and whisker plots for the AHP factors Population Density (a), Annual Rainfall (b), Drainage Density (c), Slope (d), and Land Surface Temperature (e) for the length of the Ganga contained in the area of analysis. Data distribution was tested and results are given for each factor label. Whiskers show the range of values, the box "shoulders" are the inter-quartile range, and the median is shown as a band.

S2 Fig. AHP Histogram Summary Panels (a) through (l) are the histograms and log-histograms to assess the distributions of the AHP factors along the length of the Ganga contained in the area of analysis. Panels (a), (c), (e), (g), (i) represent the histograms for Population Density, Annual Rainfall, Drainage Density, Slope, and Land Surface Temperature, respectively, while panels (b), (d), (f), (h), (j) respectively represent the log-histograms for the same. Panels (a) through (j) are binned using deciles, and coloured green to red for low to high vulnerability. (k) and (l) represent LULC and are color coded to their respective Land Use classes.

S3 Text Nested AHP pairwise comparisons and calculation

Using a pairwise comparison matrix, we assessed the relationship between individual parameter values. S4 Table shows the pairwise comparison of Population Density and the weight each category has, e.g. PD of >4036 people per km^2 has a 9 times greater effect on vulnerability than when PD was <865 people per km^2. The pairwise matrices for the other factors alongside the explanations of the comparison indices is as follows:

Minimum and maximum values for the five factor classes of population density, slope, rainfall, and drainage density were averaged, normalized, transformed to a 9-point scale to create the factor rankings, and fit to the Saaty AHP scale based on their relationships with pollution production or its transport as well as their breadth across a 9-point scale (Table 5 and S4 Table). The relationship between population density and pollution production was assumed linear based on municipal solid waste production in India [38], and the factors were ranked as 1, 4, 6, 8, and 9. Rainfall factor rankings spanned 1 through 5 on the Saaty scale because the range between lowest and highest average annual precipitation was a factor of 2 (1, 3, 4, 5, 5). Drainage density can have a nonlinear relationship with pollution transport [12], and although the range of drainage density values was more than 20-fold, its factors were ranked as 1, 6, 8, 9, and 9. The relationship between slope and transport is nonlinear for slopes greater than 26 degrees, and linear for slopes less than 26 degrees [39]. So slope factor rankings were ranked 1, 1.5, 3, 6, and 9. Minimum and maximum temperature data per factor rank were used to calculate normalized temperature dependent microbial growth rates with a Q10 (temperature coefficient) of 1.75. Then the growth rates were transformed to a 9-point scale and scored on the Saaty scale (1, 4, 5, 6, 8). LULC factor ranks were based on ESA WoldCover map [34] categories (built-up, cropland, bare/sparsely vegetated, tree cover/grassland, water/wetlands) (1,3,4,5,7). Built-up was treated as the factor rank 1 because of the breadth of pollution sources (e.g., municipal solid wastes, pathogens, excess nutrients, and heavy metals) and amount of impervious surfaces that lead to pollution transport. Cropland was ranked 3 due to runoff of fertilizers and agrochemicals. Bare/sparsely vegetated land was ranked 4 due to moderate transport risk. Tree cover and grassland were ranked 5 on the Saaty scale because these categories represent natural ecosystems, and water/wetlands were ranked as 7 on the Saaty scale, because Ganga was the point of pollution deposition.

Running AHP on this pairwise matrix for Population Density gave the subweights for classes 1 - 5. Similarly, once we ran this for the other factors; LULC, Slope, Precipitation, Drainage Density, and Temperature, we got the priority vector of subweights for each factor (S4 Table).

Table 5. Nested AHP: Priority Vector of Subweights for each factor

Factor	**AHP Weight**	**Weight of Vulnerability Classes**				
		5	**4**	**3**	**2**	**1**
Population Density	0.408	0.572	0.207	0.114	0.057	0.05
Land Use Land Cover	0.268	0.505	0.186	0.144	0.110	0.055
Slope	0.138	0.501	0.172	0.124	0.102	0.102
Precipitation	0.100	0.642	0.157	0.071	0.065	0.065
Drainage Density	0.058	0.416	0.278	0.202	0.070	0.034
Temperature	0.028	0.557	0.165	0.129	0.099	0.050

To create the vulnerability map on the Ganga buffer region using Nested AHP, we calculated the predicted vulnerability for each pixel, where:

- W is the 1x6 row vector of AHP weights:

$$W = \begin{bmatrix} w_1 & w_2 & w_3 & w_4 & w_5 & w_6 \end{bmatrix} \tag{8}$$

- $X(p)$ is the 1x6 row vector of parameter values at pixel p for the six factors:

$$X(p) = \begin{bmatrix} x_1(p) & x_2(p) & x_3(p) & x_4(p) & x_5(p) & x_6(p) \end{bmatrix} \tag{9}$$

- S is the 5x6 matrix of subweights, where each column corresponds to a factor and each row corresponds to the subweights for factor classes 1, 2, 3, 4, 5.

$$S = \begin{bmatrix} s_1(1) & s_2(1) & s_3(1) & s_4(1) & s_5(1) & s_6(1) \\ s_1(2) & s_2(2) & s_3(2) & s_4(2) & s_5(2) & s_6(2) \\ s_1(3) & s_2(3) & s_3(3) & s_4(3) & s_5(3) & s_6(3) \\ s_1(4) & s_2(4) & s_3(4) & s_4(4) & s_5(4) & s_6(4) \\ s_1(5) & s_2(5) & s_3(5) & s_4(5) & s_5(5) & s_6(5) \end{bmatrix} \tag{10}$$

Each entry $s_i(v)$ corresponds to the subweight of factor i when the value is v. For each pixel p, the parameter vector $X(p)$ is used to select corresponding subweights from S based on its value. This can be done through matrix multiplication by creating a matrix P, which will be a 5x6 binary matrix (one-hot encoded) representing the values of each parameter. For instance, if $x_1(p) = 3, x_2(p) = 1$ the matrix P will have a 1 in the corresponding positions for the values $x_1(p), x_2(p), \ldots$ at pixel p:

$$P = \begin{bmatrix} 0 & 1 & 0 & 0 & 0 & 0 \\ 0 & 0 & 0 & 0 & 1 & 0 \\ 1 & 0 & 0 & 0 & 0 & 0 \\ 0 & 0 & 1 & 0 & 0 & 0 \\ 0 & 0 & 0 & 1 & 0 & 1 \end{bmatrix} \tag{11}$$

Now, we performed the matrix multiplication between S (the subweights matrix) and P (the binary matrix).

$$S \cdot P = \begin{bmatrix} s_1(x_1(p)) & s_2(x_2(p)) & \ldots & s_6(x_6(p)) \end{bmatrix} \tag{12}$$

This operation selects the subweights corresponding to the actual values of the parameters at pixel p. Finally, we performed the dot product of the AHP weight vector W with the transpose of this resulting subweight vector $S.P$ to obtain the predicted vulnerability for each pixel using Nested AHP $V(p)$:

$$V(p) = W \cdot (S \cdot P)^T \tag{13}$$

S4 Table. Nested AHP: Factor Vulnerability Rankings for all Factors

S4 Text Fuzzy AHP calculation

In Fuzzy AHP, preferences are represented as Triangular Fuzzy Numbers (TFNs) rather than single discrete values. A triplet (l, m, u) is known as a Triangular Fuzzy Number $\tilde{A}$, where l represents the lower bound, m is the most likely value, and u is the upper bound. These numbers form a triangular shape on a graph, and they allow factors to have a range of possible values for each pairwise comparison, rather than a single exact number. For example, instead of stating that one criterion is exactly twice as important as another, a factor can be expressed such that it is “between 1.5 and 2.5 times more important, with 2 being the most likely value.” This flexibility helps to capture the subjective uncertainty inherent in human judgments.

Once we used these nonlinear weightages in our AHP calculations, we updated the map showing the different classifications of pixels based on vulnerability.

The Fuzzy Pairwise Comparison Matrix was constructed using these Triangular Fuzzy Numbers (TFN). Each element $a\ ij\tilde{a}_{ij}a\ ij$ in the matrix was a TFN representing the relative importance of criterion i over criterion j. If a criterion was compared with itself, its TFN was (1,1,1), representing absolute equality. For off-diagonal elements, if $\tilde{a}_{ij} = (l, m, u)$, then $\tilde{a}_{ji} = \left(\frac{1}{u}, \frac{1}{m}, \frac{1}{l}\right)$, maintaining the reciprocal nature of the matrix. These fuzzy comparisons were then aggregated to derive the fuzzy weight vector for each criterion.

In Fuzzy AHP, the decision maker generally recreates the pairwise matrix by choosing the l, m, u for each element, but to understand the outlying cases for Fuzzy AHP, and to incorporate the breadth of decision maker's range, we ran Fuzzy AHP on 100,000 Monte Carlo simulations at 95% fuzziness. For each run, we made a unique Fuzzy Pairwise Comparison Matrix, where if the comparison index between two factors was 2, the triangular fuzzy range would be $(0.05 * 2, 2, 2 * 1.95) = (0.1, 2, 3.9)$, and we chose a random value between 0.1 and 2, and 2 and 3.9 to design the final TFN

$[random.uniform(0.1, 2), 2, random.uniform(2, 3.9)]$. Running 100,000 simulations took into account most of the likely Fuzzy Pairwise Comparison Matrices that might be generated.

We ran Fuzzy AHP on each Fuzzy Pairwise Comparison Matrix, where we calculated the geometric mean across each row of the matrix, and normalized the results. The final step was to defuzzify these fuzzy numbers by taking the mean, which returned the priority vector. We then determined the number of cases out of 100,000 where there were rank reversals. We observed the cases where the order of parameters in terms of vulnerability changed, as compared to rank-orders in case of classic AHP.

S5 Text ANP supermatrix and inner dependence (W22 and W33) pairwise comparisons Pairwise comparisons were made to describe the relative importance of the ANP criteria (AHP factors) on influencing each other (S3 Fig). Criteria that did not contribute to an inner dependence matrix were scored with a zero. When identifying the relative importance of Land Use Land Cover (LULC) compared to other criteria on influencing Population Density (PD), it was scored with a 2 because of the importance of built-up and agriculture categories in LULC and their direct relationships with population densities. Rainfall and slope were scored with a 5 because historically there were natural limits to both that influenced urbanization and agriculture although this is changing [40; 41; 42; 43; 44]. Drainage Density (DD) was scored an 8 because the natural drainage density is modified by people to meet agricultural and societal requirements suggesting it has a minor influence on PD. When identifying the relative importance of PD compared to other criteria on influencing LULC, it was scored with a 2 as a reciprocal of the LULC-PD inner dependence. Rainfall and temperature are major drivers of land cover type, and as such each was scored with a 4. Slope and DD shape landscapes within land cover types, and each was scored with a 7. When identifying the relative importance of LULC compared to other criteria on influencing rainfall, it was scored with a 7 and PD was scored with an 8 because of the potential for built-up land to influence local precipitation [45]. Slope may influence the speed of runoff during rainfall and was scored with a 5. When identifying the relative importance of criteria on influencing DD, PD was scored a 2, LULC was scored a 4, and slope was scored a 7, because DD is the product of both anthropogenic and natural influences. When identifying the relative importance of criteria on influencing temperature, PD was scored a 5, and LULC was scored an 8 to account for potential urban heat island effects.

S3 Fig. ANP Parameter Inner Dependencies Inner dependencies between ANP criteria (AHP factors) are shown as ovals. Arrows about the ovals indicate influence by a criterion on other criteria to its right and arrows below the ovals indicate influence by a criterion on other criteria to its left.

S6 Text 1-N AHP calculation

We first took our original output of AHP, i.e. the weights of the known factors. Here, we assumed that our known factors would at least represent 67% of the importance while classifying the vulnerability variable. This is a fair assumption since through our preliminary analysis we can conclude that our factors were robust enough to represent at least 67% of the variability of the vulnerability variable.

The unknown factors could be one of two types: acute or chronic. Some factors (acute) may be less likely to occur but more likely to have a significant impact on vulnerability, while other factors (chronic) may be more likely to occur but less likely to have a less significant impact. In the case of our problem statement, acute factors might include mining sites and hide tanning operations while chronic factors might include algal blooms from fertilizer runoff and pollution during funeral processions.

To assess the potential impact of these acute and chronic factors, we first created two new layers on the river Ganga buffer region, with uniformly distributed random values from 1-5 similar to the other factors, and pixels with value zero, to capture the probabilistic non-occurrence of acute or chronic factors. For chronic factors, 75% of the pixels were 0, while for acute factors 97.5% of the pixels were 0. This means that each variable had a 25% and a 2.5% probability of occurrence respectively, where pixels were assigned the random values 1-5.

To evaluate the unknown variability captured between 1-N (where N lies between 0.67 and 1), we split it between acute and chronic. We assumed that since acute factors have a significant impact on vulnerability, 90% of the 1-N factor would be attributed to the impact of acute factors to vulnerability, while the leftover 10% would be attributed to the impact of chronic factors to vulnerability. For instance, in the worst case scenario if 1-N is 0.33 (i.e. the weightage of the unknown factors towards vulnerability is 33%), the 0.33 will be split into 0.297 for acute and 0.033 for chronic. The original six factors, with their weights 0.408, 0.268, 0.138, 0.100, 0.058, 0.028 will be scaled down based on N. If N is 0.67, we multiply the old weights by 0.67 so that they sum up to n, and we can accommodate the new acute and chronic weights. Here, 0.408*0.67 gives 0.27336, which would be lower than 0.297 for acute factors, which means the acute factors would have a higher impact on vulnerability but with a lower probability.

We ran AHP using the original six layers and two additional layers, with new weights to accommodate for acute and chronic factors, and compared the results with the AHP results to check the robustness of our model. We ran this approach once with 1-N as 0.33 to represent a worst case scenario, and once with 1-N as 0.165 to reflect the average or expected case.

To ensure consistent results while dealing with abstract foundations for parameter understanding, we performed our analysis on a set of assumptions. We assumed that our classic AHP model at least represented 67% of the importance in terms of weights and that the value of 1-N could be anything between 0 and 0.33 with a uniform distribution. Also, to deal with the uncertainty, we assumed that the unknown factors can be of two types - acute and chronic, with a 2.5% and a 25% probability of occurrence respectively; and while there could be numerous unknown factors, they can be clumped into two factors - acute and chronic. Lastly, we assumed that the non-zero pixel values were randomly and uniformly distributed with their appropriate probabilities.

S4 Fig. ANP with original AHP submatrix These figures show the ANP's vulnerability score with the original AHP submatrix; the lower values pertained to the least vulnerable areas while the ones with higher scores were the most vulnerable. Map of exact values per pixel location (a) and histogram of binned ranges of values (b).

S5 Fig. Original AHP & AHP Variants Comparison Chart These figures show the comparison charts for the different variants of AHP with the original AHP across the Ganga buffer. We used three map types to highlight the distribution of differences between the approaches. Column (a) is Map type 1 (colors spread between overall min max), Column (b) is Map type 2 (colors spread between local min max), and Column (c) is Map type 3 (colors spread between 5-95 percentile). Rows 1-8 are Nested AHP, ANP, 1-N AHP (Worst case), 1-N AHP (Avg case), Fuzzy AHP (Mean), Fuzzy AHP (Case1), Fuzzy AHP (Case2) and Population density, respectively.

Author contributions

Conceptualization: Sarthak Arora, James C. Smoot, Nikhil Raj Deep, Claire Gorman Hanly, Anthony Acciavatti.

Data curation: Sarthak Arora, Michael Warner, Ariel Chamberlain.
Formal analysis: Sarthak Arora, Ariel Chamberlain.
Investigation: Sarthak Arora.
Methodology: Sarthak Arora.
Project administration: James C. Smoot, Anthony Acciavatti.
Supervision: James C. Smoot, Anthony Acciavatti.
Visualization: Sarthak Arora, Michael Warner, Ariel Chamberlain.
Writing – original draft: Sarthak Arora, Michael Warner, James C. Smoot.
Writing – review & editing: Sarthak Arora, Michael Warner, Ariel Chamberlain, James C. Smoot, Nikhil Raj Deep, Claire Gorman Hanly, Anthony Acciavatti.

Acknowledgments

The authors thank Markley Boyer and Sarah Bergmann for thoughtful discussions throughout the project. We also thank Aaron Hirsh for organizing Collaborative Earth.

References

1. Simon M, Joshi H. Story of the Ganga River: Its Pollution and Rejuvenation. *Riverine Systems*. pp. 21-55 (2022), https://link.springer.com/10.1007/978-3-030-87067-6_2

2. Modi A, Bhagat C, Mohapatra P. Impact of Urbanization on Ganga River Basin: An Overview in the Context of Natural Surface Water Resources. *Impacts Of Urbanization On Hydrological Systems In India*. pp. 111-127 (2023), https://link.springer.com/10.1007/978-3-031-21618-3_6

3. Sharma N, Liang M, Laskar A, Huang K, Maurya N, Singh V, Ranjan R, Maurya A. Basin-Scale Geochemical Assessment of Water Quality in the Ganges River during the Dry Season. *Water*. **15**, 2026 (2023,5), https://www.mdpi.com/2073-4441/15/11/2026

4. Srinivas R, Singh A, Shankar D. Understanding the threats and challenges concerning Ganges River basin for effective policy recommendations towards sustainable development. *Environ. Dev. Sustain.*. **22**, 3655-3690 (2020,4), http://link.springer.com/10.1007/s10668-019-00361-0

5. Pal P. Arth Ganga: A Sustainable Model for Ganga River Rejuvenation. *A Basic Overview Of Environment And Sustainable Development [Volume 2]*. pp. 138-154 (2023), https://books.iaph.in/chapter-9-arth-ganga-a-sustainable-model-for-ganga-river-rejuvenation/

6. Plummer R, De Loë R, Armitage D. A Systematic Review of Water Vulnerability Assessment Tools. *Water. Resour. Manage.*. **26**, 4327-4346 (2012,12), http://link.springer.com/10.1007/s11269-012-0147-5

7. Saaty T. The Analytic Hierarchy Process: Planning, Priority Setting, Resource Allocation. (McGraw-Hill International Book Company,1980), https://books.google.co.uk/books?id=Xxi7AAAAIAAJ

8. Jhariya D, Khan R, Mondal K, Kumar T, K I, Singh V. Assessment of groundwater potential zone using GIS-based multi-influencing factor (MIF), multi-criteria decision analysis (MCDA) and electrical resistivity survey techniques in Raipur city, Chhattisgarh, India. *J. Water. Supply. Res. T.*. **70**,

375-400 (2021,5),
https://iwaponline.com/aqua/article/70/3/375/80608/Assessment-of-groundwater-potential-zone-using-GIS

9. Liu C, Chen J, Shan X, Yang Y, Song L, Teng Y, Chen H. Meta-analysis addressing the characterization and risk identification of antibiotics and antibiotic resistance genes in global groundwater. *Sci. Total. Environ.*. **860** pp. 160513 (2023,2), https://linkinghub.elsevier.com/retrieve/pii/S004896972207615X

10. Yu S, Xu Z, Wu W, Zuo D. Effect of land use types on stream water quality under seasonal variation and topographic characteristics in the Wei River basin, China. *Ecol. Indic.*. **60** pp. 202-212 (2016,1), https://linkinghub.elsevier.com/retrieve/pii/S1470160X15003623

11. Nobre R, Caliman A, Cabral C, Araújo F, Guérin J, Dantas F, Quesado L, Venticinque E, Guariento R, Amado A, Kelly P, Vanni M, Carneiro L. Precipitation, landscape properties and land use interactively affect water quality of tropical freshwaters. *Sci. Total. Environ.*. **716** pp. 137044 (2020,5), https://linkinghub.elsevier.com/retrieve/pii/S0048969720305544

12. Bedient P, Heaney J, Huber W. Drainage Density as Index of Watershed Development. *J. Irrig. And Drain. Div.*. **104**, 373-387 (1978,12), https://ascelibrary.org/doi/10.1061/JRCEA4.0001220

13. Ferral A, German A, Beltramone G, Bonansea M, Burgos P, De Carvalho L, Michal S, Roque M, Scavuzzo M. Spatio-Temporal Analysis of Water Surface Temperature in a Reservoir and its Relation with Water Quality in a Climate Change Context. *2021 IEEE Int. Geosci. Remote. Se.*. pp. 76-79 (2021,7), https://ieeexplore.ieee.org/document/9553255/

14. Smoot J, Findlay R. Spatial and Seasonal Variation in a Reservoir Sedimentary Microbial Community as Determined by Phospholipid Analysis. *Microbial. Ecol.*. **42**, 350-358 (2001,10), http://link.springer.com/10.1007/s002480000102

15. Munier N, Hontoria E. Shortcomings of the AHP Method. *Uses And Limitations Of The AHP Method*. pp. 41-90 (2021), http://link.springer.com/10.1007/978-3-030-60392-2_5, Series Title: Management for Professionals

16. Saaty T. The Analytic Network Process. *Decision Making With The Analytic Network Process*. **95** pp. 1-26 (2006), http://link.springer.com/10.1007/0-387-33987-6_1, Series Title: International Series in Operations Research Management Science

17. Saaty T. The Analytic Hierarchy Process: A New Approach to Deal with Fuzziness in Architecture. *Archit. Sci. Rev.*. **25**, 64-69 (1982,9), http://www.tandfonline.com/doi/abs/10.1080/00038628.1982.9696499

18. Rahaman S, Ajeez S, Aruchamy S, Jegankumar R. Prioritization of Sub Watershed Based on Morphometric Characteristics Using Fuzzy Analytical Hierarchy Process and Geographical Information System – A Study of Kallar Watershed, Tamil Nadu. *Aquat. Pr.*. **4** pp. 1322-1330 (2015), https://linkinghub.elsevier.com/retrieve/pii/S2214241X1500173X

19. Jenks G, Caspall F. Error on Choroplethic Maps: Definition, Measurement, Reduction. *Ann. Assoc. Am. Geogr.*. **61**, 217-244 (1971,6), http://www.tandfonline.com/doi/abs/10.1111/j.1467-8306.1971.tb00779.x

20. Poh K, Liang Y. Multiple-Criteria Decision Support for a Sustainable Supply Chain: Applications to the Fashion Industry. *Informatics.* **4**, 36 (2017,10), https://www.mdpi.com/2227-9709/4/4/36

21. Adams, B, Elena & Badger, T. wjladams/pyanp: Minor additions. (Zenodo,2020,4), https://zenodo.org/record/3774063

22. Bayazidy M, Maleki M, Khosravi A, Shadjou A, Wang J, Rustum R, Morovati R. Assessing Riverbank Change Caused by Sand Mining and Waste Disposal Using Web-Based Volunteered Geographic Information. *Water.* **16**, 734 (2024,2), https://www.mdpi.com/2073-4441/16/5/734

23. Dinerstein E, Joshi A, Hahn N, Lee A, Vynne C, Burkart K, Asner G, Beckham C, Ceballos G, Cuthbert R, Dirzo R, Fankem O, Hertel S, Li B, Mellin H, Pharand-Deschênes F, Olson D, Pandav B, Peres C, Putra R, Rosenthal A, Verwer C, Wikramanayake E, Zolli A. Conservation Imperatives: securing the last unprotected terrestrial sites harboring irreplaceable biodiversity. *Front. Sci..* **2** pp. 1349350 (2024,6), https://www.frontiersin.org/articles/10.3389/fsci.2024.1349350/full

24. Yang Y, Song W, Lin H, Wang W, Du L, Xing W. Antibiotics and antibiotic resistance genes in global lakes: A review and meta-analysis. *Environ. Int..* **116** pp. 60-73 (2018,7), https://linkinghub.elsevier.com/retrieve/pii/S0160412017320238

25. Loi D. Assessment of Urban Flood Vulnerability Using Integrated Multi-parametric AHP and GIS. *IJG.* (2023,6), https://journals.sfu.ca/ijg/index.php/journal/article/view/2689

26. Tripathi R, Ramachandran A, Tripathi V, Badola R, Hussain S. Optimizing Riparian Habitat Conservation: A Spatial Approach Using Aerial and Space Technologies. *IEEE J. Sel. Top. Appl. Earth Observations Remote Sensing.* **17** pp. 16932-16943 (2024), https://ieeexplore.ieee.org/document/10664440/

27. Zhou T, Ren W, Peng S, Liang L, Ren S, Wu J. A riverscape transect approach to studying and restoring river systems: A case study from southern China. *Ecol. Eng..* **65** pp. 147-158 (2014,4), https://linkinghub.elsevier.com/retrieve/pii/S0925857413003480

28. Das S, Gupta A. Multi-criteria decision based geospatial mapping of flood susceptibility and temporal hydro-geomorphic changes in the Subarnarekha basin, India. *Geosci. Front..* **12**, 101206 (2021,9), https://linkinghub.elsevier.com/retrieve/pii/S1674987121000700

29. Liyanage C, Yamada K. Impact of Population Growth on the Water Quality of Natural Water Bodies. *Sustainability.* **9**, 1405 (2017,8), https://www.mdpi.com/2071-1050/9/8/1405

30. Nguyen H, Fukuda H, Nguyen M. Assessment of the Susceptibility of Urban Flooding Using GIS with an Analytical Hierarchy Process in Hanoi, Vietnam. *Sustainability.* **16**, 3934 (2024,5), https://www.mdpi.com/2071-1050/16/10/3934

31. Withanage N, Gunathilaka K, Mishra P, Abdelrahman K, Wijesinghe D, Mishra V, Tripathi S, S. Fnais M. A quality of life index for the rural periphery of Sri Lanka using GIS multi-criteria decision analysis techniques. *PLoS ONE.* **19**, e0308077 (2024,9), https://dx.plos.org/10.1371/journal.pone.0308077

32. Steele K, Carmel Y, Cross J, Wilcox C. Uses and Misuses of Multicriteria Decision Analysis (MCDA) in Environmental Decision Making. *Risk Anal.*. **29**, 26-33 (2009,1), https://onlinelibrary.wiley.com/doi/10.1111/j.1539-6924.2008.01130.x

33. NASA JPL NASADEM Merged DEM Global 1 arc second V001. (NASA EOSDIS Land Processes Distributed Active Archive Center,2020), https://lpdaac.usgs.gov/products/nasadem_hgtv001

34. Zanaga D, Van De Kerchove R, Daems D, De Keersmaecker W, Brockmann C, Kirches G, Wevers J, Cartus O, Santoro M, Fritz S, Lesiv M, Herold M, Tsendbazar N, Xu P, Ramoino F, Arino O. ESA WorldCover 10 m 2021 v200. (Zenodo,2022,10), https://zenodo.org/record/7254221

35. Center For International Earth Science Information Network-CIESIN-Columbia University Gridded Population of the World, Version 4 (GPWv4): Population Density Adjusted to Match 2015 Revision UN WPP Country Totals, Revision 11. (Palisades, NY: NASA Socioeconomic Data,2018), https://earthdata.nasa.gov/data/catalog/sedac-ciesin-sedac-gpwv4-apdens-wpp-2015-r11-4.11

36. Funk C, Peterson P, Landsfeld M, Pedreros D, Verdin J, Shukla S, Husak G, Rowland J, Harrison L, Hoell A, Michaelsen J. The climate hazards infrared precipitation with stations—a new environmental record for monitoring extremes. *Sci. Data.*. **2**, 150066 (2015,12), https://www.nature.com/articles/sdata201566

37. USGS Landsat 8 Level 2, Collection 2, Tier 1, courtesy of the U.S. Geological Survey.

38. Goel S. Municipal solid waste management (MSWM) in India: a critical review. *J. Environ. Sci. Eng.*. **50**, 319-328 (2008,10)

39. Andrews D, Bucknam R. Fitting degradation of shoreline scarps by a nonlinear diffusion model. *J. Geophys. Res.*. **92**, 12857-12867 (1987,11), https://agupubs.onlinelibrary.wiley.com/doi/10.1029/JB092iB12p12857

40. Zhou L, Dang X, Mu H, Wang B, Wang S. Cities are going uphill: Slope gradient analysis of urban expansion and its driving factors in China. *Sci. Total. Environ.*. **775** pp. 145836 (2021,6), https://linkinghub.elsevier.com/retrieve/pii/S0048969721009037

41. Chen H, Tan Y, Xiao W, Li G, Meng F, He T, Li X. Urbanization in China drives farmland uphill under the constraint of the requisition–compensation balance. *Sci. Total. Environ.*. **831** pp. 154895 (2022,7), https://linkinghub.elsevier.com/retrieve/pii/S004896972201988X

42. Shi K, Wu Y, Liu S. Slope climbing of urban expansion worldwide: Spatiotemporal characteristics, driving factors and implications for food security. *J. Environ. Manage.*. **324** pp. 116337 (2022,12), https://linkinghub.elsevier.com/retrieve/pii/S0301479722019107

43. Wang H, Liu Y, Wang Y, Yao Y, Wang C. Land cover change in global drylands: A review. *Sci. Total. Environ.*. **863** pp. 160943 (2023,3), https://linkinghub.elsevier.com/retrieve/pii/S0048969722080469

44. Ullah S, Shi Y, Dasti M, Wajid M, Saqib Z. Estimating Advance of Built-Up Area in Desert-Oasis Ecotone of Cholistan Desert Using Landsat. *Land*. **12**, 1009 (2023,5), https://www.mdpi.com/2073-445X/12/5/1009

45. Liu J, Niyogi D. Meta-analysis of urbanization impact on rainfall modification. *Sci. Rep.*. **9**, 7301 (2019,5), https://www.nature.com/articles/s41598-019-42494-2


Kabul
Islamabad
HANISTAN
PLATEAU OF TIBET
Yangtze
Mekong
Indus
Salween
Lahore
Brahmaputra
PAKISTAN
New Delhi
NEPAL
Ganges
Karachi
Ahmedabad
INDIA
BANGLADESH
Dhaka
MYANMAR (BURMA)
Mumbai
Pune
Hyderabad
Yangon
THAI
Bengaluru
Chennai
Bangkok
Phnom
LANKA
Colombo
0 375 750 1,500 KM
Esri, HERE, Garmin, FAO, NOAA, USGS
Dehradun
UTTARAKHAND
Muzaffarnagar
Meerut
Moradabad
Rampur
Ghaziabad
Bulandshahr
Bareilly
Budaun
Aligarh
Shahjahanpur
Lakhimpur
Mathura
Sitapur
Bahraich
Agra
Firozabad
Etawah
UTTAR PRADESH
Lucknow
Faizabad
Gorakhpur
Kanpur
Gwalior
Rae Bareli
Orai
Fatehpur
Yamuna
Betwa
Maunath Bhanjan
Jaunpur
Shivpuri
Banda
Allahabad
Varanasi
Jhansi
Mirzapur cum Vindhyachal
Sasaram
Gaya
Rewa
Son
Patna
Arrah
Muzaffar
Bettiah
Birganj
Kathman
Pokhara
NEPAL
Gandaki Nadi
Ghaghra
Annapurna Conservation Area
Manaslu Conservation Area
She Phoksundo National Park
Nanda Devi National Park
Royal Chitawan National Park
0 70 140 280 420 KM
Esri, HERE, Garmin, FAO, USGS

Fig1

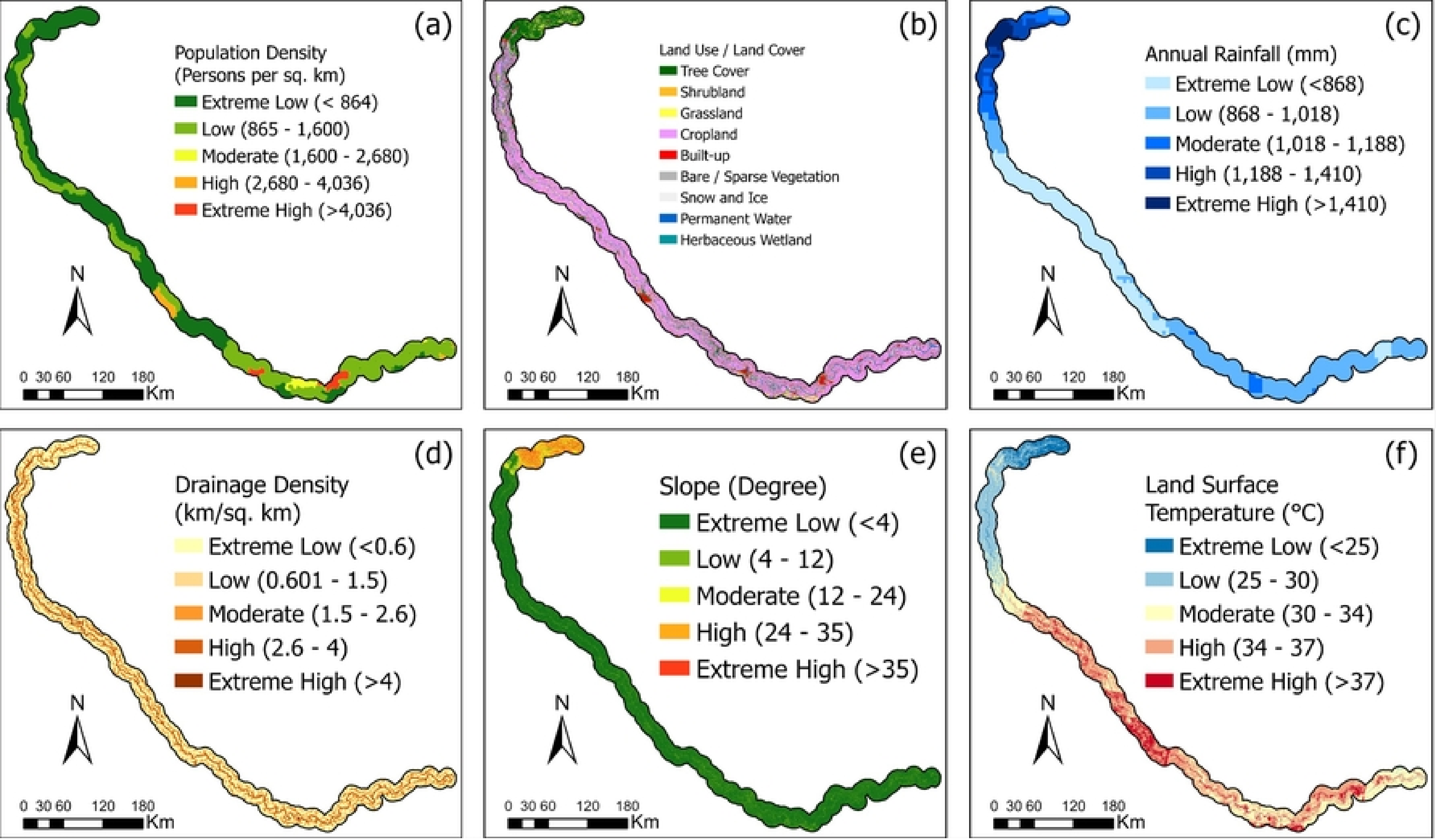
(a)
Population Density
(Persons per sq. km)
Extreme Low (< 864)
Low (865 - 1,600)
Moderate (1,600 - 2,680)
High (2,680 - 4,036)
Extreme High (>4,036)
(b)
Land Use / Land Cover
Tree Cover
Shrubland
Grassland
Cropland
Built-up
Bare / Sparse Vegetation
Snow and Ice
Permanent Water
Herbaceous Wetland
(c)
Annual Rainfall (mm)
Extreme Low (<868)
Low (868 - 1,018)
Moderate (1,018 - 1,188)
High (1,188 - 1,410)
Extreme High (>1,410)
(d)
Drainage Density
(km/sq. km)
Extreme Low (<0.6)
Low (0.601 - 1.5)
Moderate (1.5 - 2.6)
High (2.6 - 4)
Extreme High (>4)
(e)
Slope (Degree)
Extreme Low (<4)
Low (4 - 12)
Moderate (12 - 24)
High (24 - 35)
Extreme High (>35)
(f)
Land Surface
Temperature (°C)
Extreme Low (<25)
Low (25 - 30)
Moderate (30 - 34)
High (34 - 37)
Extreme High (>37)
N
0 30 60 120 180
Km

Fig2

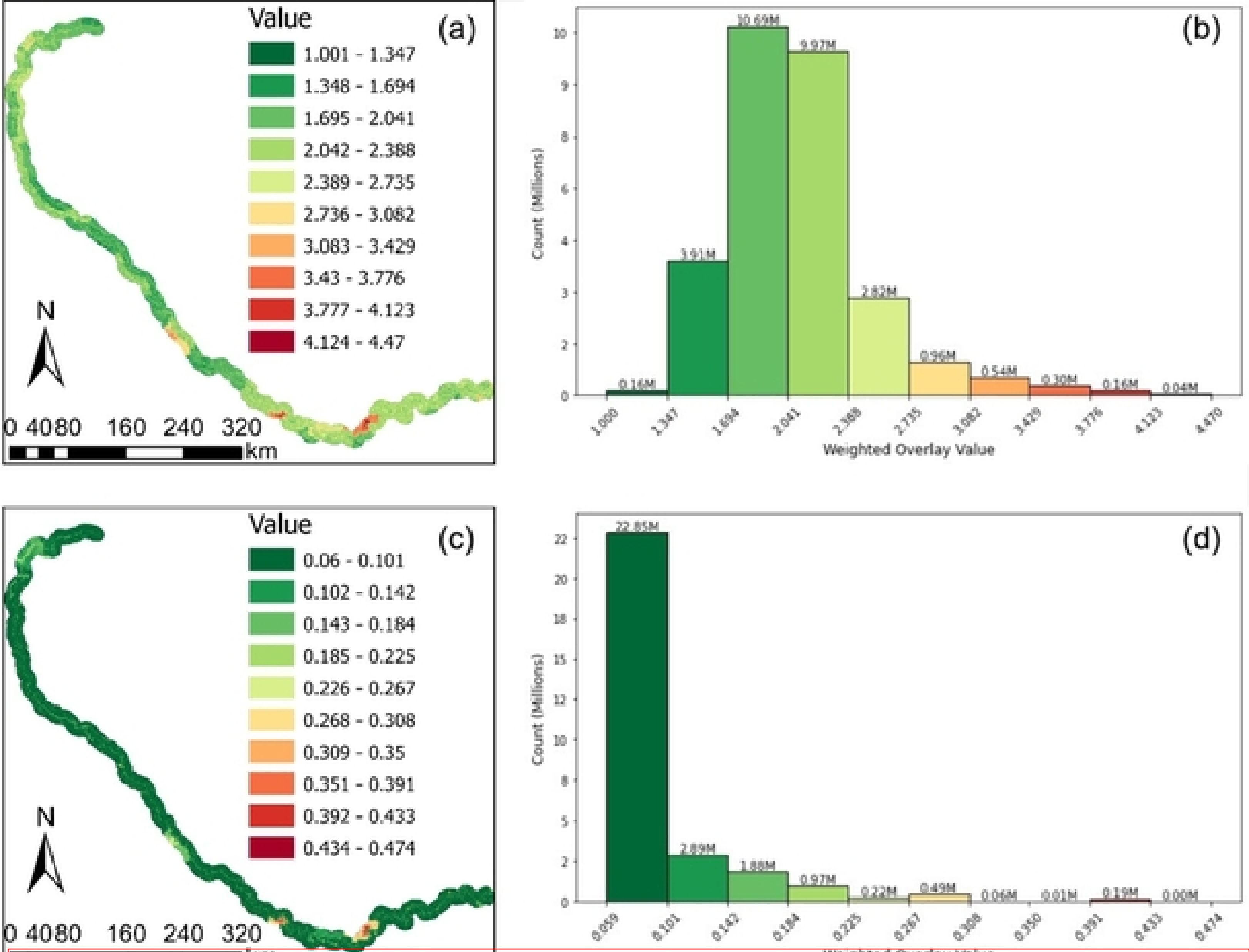

Value
1.001 - 1.347
1.348 - 1.694
1.695 - 2.041
2.042 - 2.388
2.389 - 2.735
2.736 - 3.082
3.083 - 3.429
3.43 - 3.776
3.777 - 4.123
4.124 - 4.47
(a)
N
0 4080 160 240 320
km
(b)
Count (Millions)
0.16M
3.91M
10.69M
9.97M
2.82M
0.96M
0.54M
0.30M
0.16M
0.04M
1.000 1.347 1.694 2.041 2.388 2.735 3.082 3.429 3.776 4.123 4.470
Weighted Overlay Value
Value
0.06 - 0.101
0.102 - 0.142
0.143 - 0.184
0.185 - 0.225
0.226 - 0.267
0.268 - 0.308
0.309 - 0.35
0.351 - 0.391
0.392 - 0.433
0.434 - 0.474
(c)
N
0 4080 160 240 320
km
(d)
Count (Millions)
22.85M
2.89M
1.88M
0.97M
0.22M
0.49M
0.06M
0.01M
0.19M
0.00M
0.059 0.101 0.142 0.184 0.225 0.267 0.308 0.350 0.391 0.433 0.474
Weighted Overlay Value

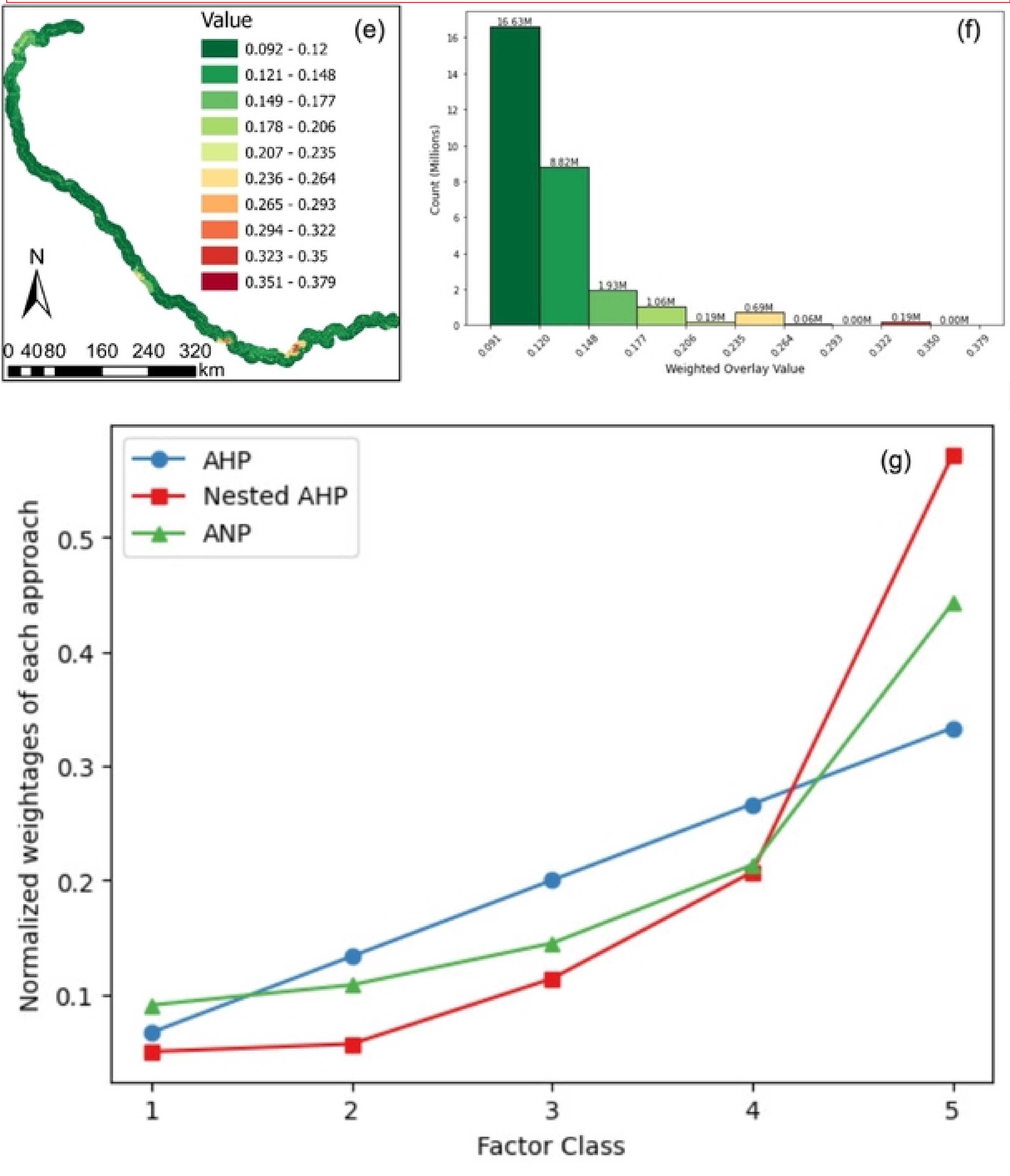

Value
0.092 - 0.12
0.121 - 0.148
0.149 - 0.177
0.178 - 0.206
0.207 - 0.235
0.236 - 0.264
0.265 - 0.293
0.294 - 0.322
0.323 - 0.35
0.351 - 0.379
(e)
N
0 4080 160 240 320
km
(f)
Count (Millions)
16.63M
8.82M
1.93M
1.06M
0.19M
0.69M
0.06M
0.00M
0.19M
0.00M
0.091 0.120 0.148 0.177 0.206 0.235 0.264 0.293 0.322 0.350 0.379
Weighted Overlay Value
AHP
Nested AHP
ANP
(g)
Normalized weightages of each approach
Factor Class

Fig3

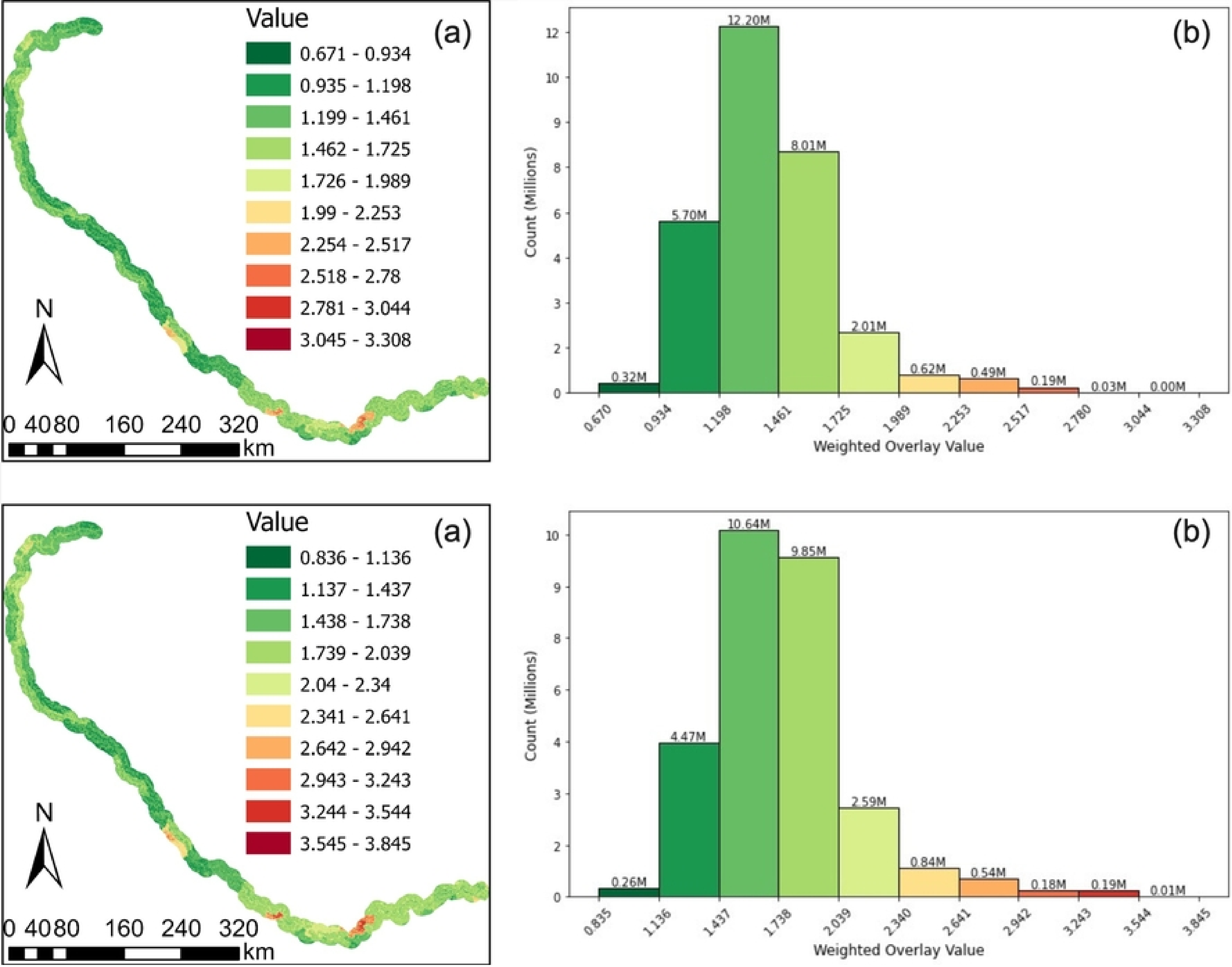
Value
(a)
0.671 - 0.934
0.935 - 1.198
1.199 - 1.461
1.462 - 1.725
1.726 - 1.989
1.99 - 2.253
2.254 - 2.517
2.518 - 2.78
2.781 - 3.044
3.045 - 3.308
N
0 40 80 160 240 320
km
(b)
Count (Millions)
Weighted Overlay Value
0.32M
5.70M
12.20M
8.01M
2.01M
0.62M
0.49M
0.19M
0.03M
0.00M
0.670
0.934
1.198
1.461
1.725
1.989
2.253
2.517
2.780
3.044
3.308
Value
(a)
0.836 - 1.136
1.137 - 1.437
1.438 - 1.738
1.739 - 2.039
2.04 - 2.34
2.341 - 2.641
2.642 - 2.942
2.943 - 3.243
3.244 - 3.544
3.545 - 3.845
N
0 40 80 160 240 320
km
(b)
Count (Millions)
Weighted Overlay Value
0.26M
4.47M
10.64M
9.85M
2.59M
0.84M
0.54M
0.18M
0.19M
0.01M
0.835
1.136
1.437
1.738
2.039
2.340
2.641
2.942
3.243
3.544
3.845

Fig4

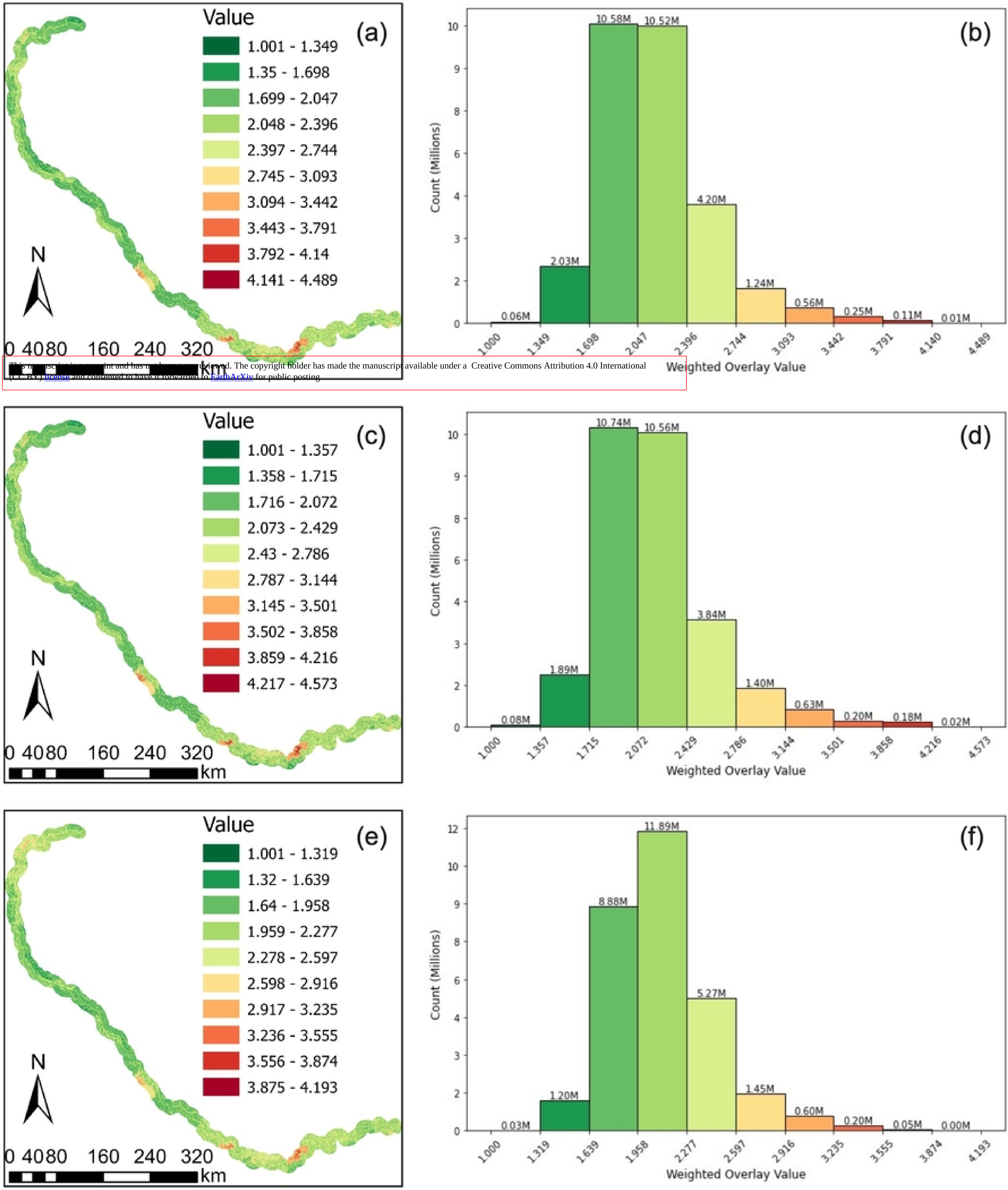
(a)
Value
1.001 - 1.349
1.35 - 1.698
1.699 - 2.047
2.048 - 2.396
2.397 - 2.744
2.745 - 3.093
3.094 - 3.442
3.443 - 3.791
3.792 - 4.14
4.141 - 4.489
N
0 40 80 160 240 320
km
(b)
Count (Millions)
Weighted Overlay Value
0.06M
2.03M
10.58M
10.52M
4.20M
1.24M
0.56M
0.25M
0.11M
0.01M
1.000 1.349 1.698 2.047 2.396 2.744 3.093 3.442 3.791 4.140 4.489
(c)
Value
1.001 - 1.357
1.358 - 1.715
1.716 - 2.072
2.073 - 2.429
2.43 - 2.786
2.787 - 3.144
3.145 - 3.501
3.502 - 3.858
3.859 - 4.216
4.217 - 4.573
N
0 40 80 160 240 320
km
(d)
Count (Millions)
Weighted Overlay Value
0.08M
1.89M
10.74M
10.56M
3.84M
1.40M
0.63M
0.20M
0.18M
0.02M
1.000 1.357 1.715 2.072 2.429 2.786 3.144 3.501 3.858 4.216 4.573
(e)
Value
1.001 - 1.319
1.32 - 1.639
1.64 - 1.958
1.959 - 2.277
2.278 - 2.597
2.598 - 2.916
2.917 - 3.235
3.236 - 3.555
3.556 - 3.874
3.875 - 4.193
N
0 40 80 160 240 320
km
(f)
Count (Millions)
Weighted Overlay Value
0.03M
1.20M
8.88M
11.89M
5.27M
1.45M
0.60M
0.20M
0.05M
0.00M
1.000 1.319 1.639 1.958 2.277 2.597 2.916 3.235 3.555 3.874 4.193

Fig5

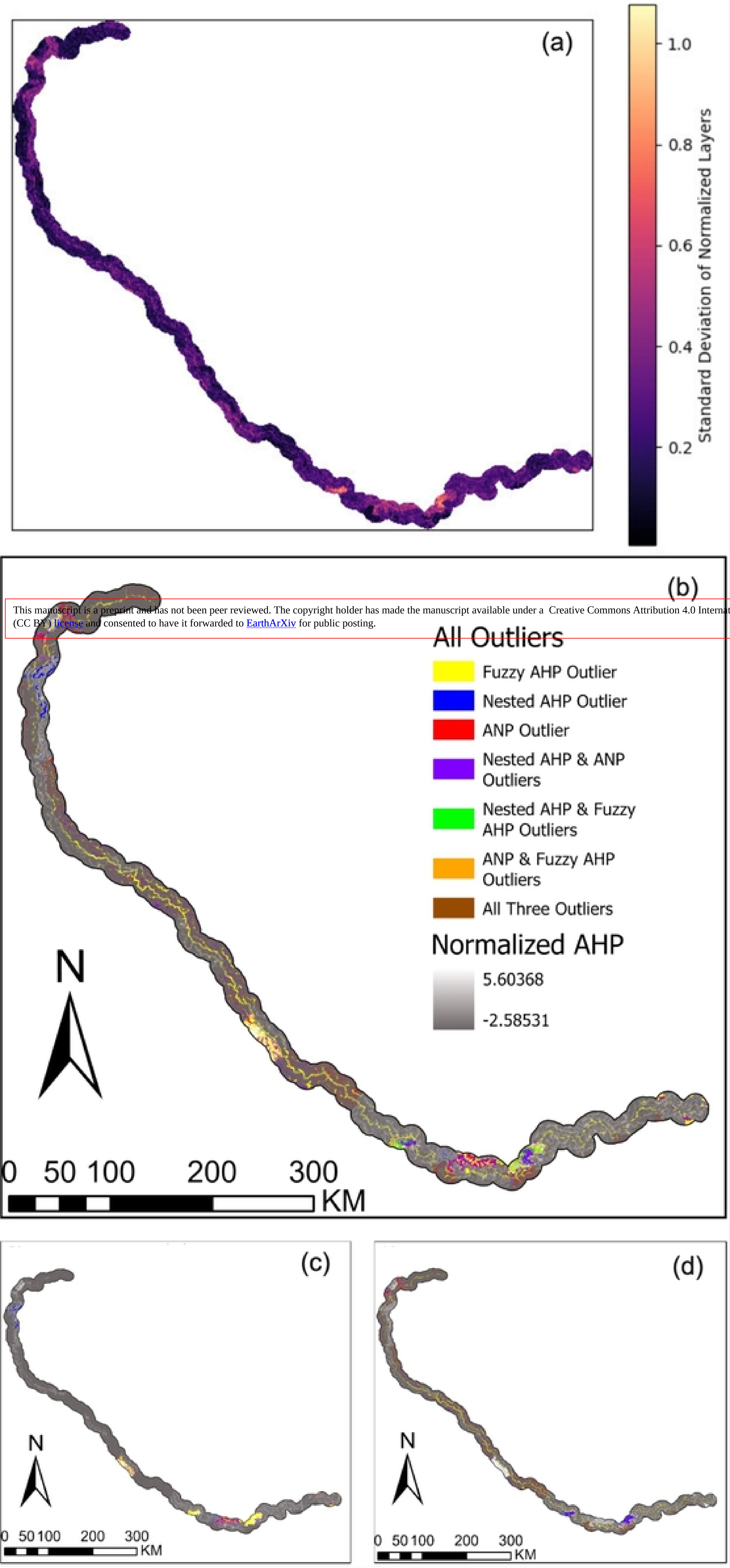
(a)
1.0
0.8
0.6
0.4
0.2
Standard Deviation of Normalized Layers
(b)
All Outliers
Fuzzy AHP Outlier
Nested AHP Outlier
ANP Outlier
Nested AHP & ANP Outliers
Nested AHP & Fuzzy AHP Outliers
ANP & Fuzzy AHP Outliers
All Three Outliers
Normalized AHP
5.60368
-2.58531
N
0 50 100 200 300
KM
(c)
N
0 50 100 200 300
KM
(d)
N
0 50 100 200 300
KM

Fig6

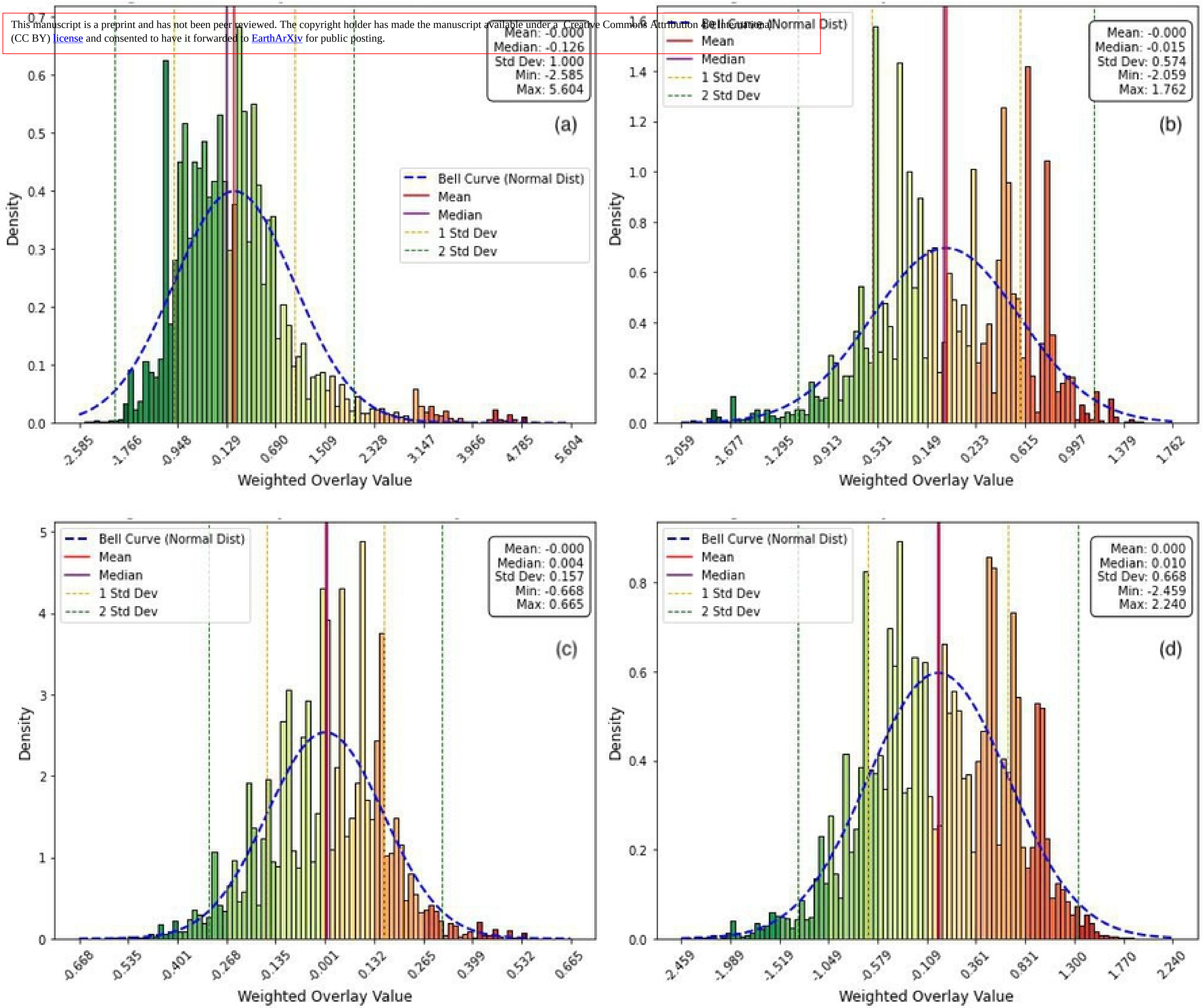
(a)
Mean: -0.000
Median: -0.126
Std Dev: 1.000
Min: -2.585
Max: 5.604
Bell Curve (Normal Dist)
Mean
Median
1 Std Dev
2 Std Dev
Density
Weighted Overlay Value
-2.585 -1.766 -0.948 -0.129 0.690 1.509 2.328 3.147 3.966 4.785 5.604
(b)
Mean: -0.000
Median: -0.015
Std Dev: 0.574
Min: -2.059
Max: 1.762
-2.059 -1.677 -1.295 -0.913 -0.531 -0.149 0.233 0.615 0.997 1.379 1.762
(c)
Mean: -0.000
Median: 0.004
Std Dev: 0.157
Min: -0.668
Max: 0.665
-0.668 -0.535 -0.401 -0.268 -0.135 -0.001 0.132 0.265 0.399 0.532 0.665
(d)
Mean: 0.000
Median: 0.010
Std Dev: 0.668
Min: -2.459
Max: 2.240
-2.459 -1.989 -1.519 -1.049 -0.579 -0.109 0.361 0.831 1.300 1.770 2.240

Fig7

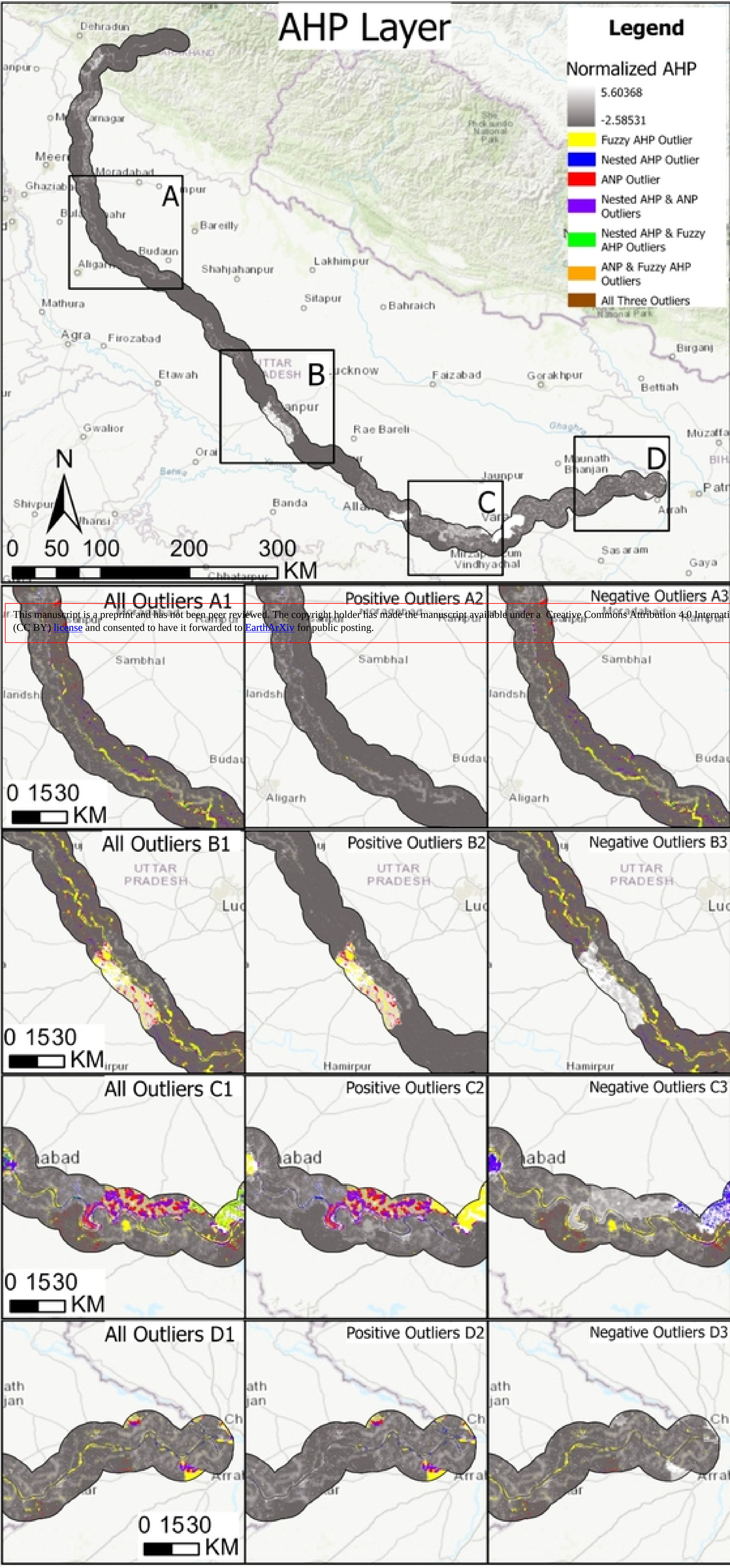
AHP Layer
Legend
Normalized AHP
5.60368
-2.58531
Fuzzy AHP Outlier
Nested AHP Outlier
ANP Outlier
Nested AHP & ANP Outliers
Nested AHP & Fuzzy AHP Outliers
ANP & Fuzzy AHP Outliers
All Three Outliers
A
B
C
D
N
0 50 100 200 300
KM
Dehradun
Moradabad
Bareilly
Budaun
Aligarh
Shahjahanpur
Lakhimpur
Sitapur
Bahraich
Mathura
Agra
Firozabad
Etawah
Lucknow
Faizabad
Gorakhpur
Bettiah
Birganj
Gwalior
Rae Bareli
Jaunpur
Banda
Shivpuri
Sasaram
Gaya
Arrah
Muzaffa
All Outliers A1
Positive Outliers A2
Negative Outliers A3
Sambhal
Aligarh
0 1530
KM
All Outliers B1
Positive Outliers B2
Negative Outliers B3
UTTAR PRADESH
Hamirpur
0 1530
KM
All Outliers C1
Positive Outliers C2
Negative Outliers C3
0 1530
KM
All Outliers D1
Positive Outliers D2
Negative Outliers D3
0 1530
KM

Fig8

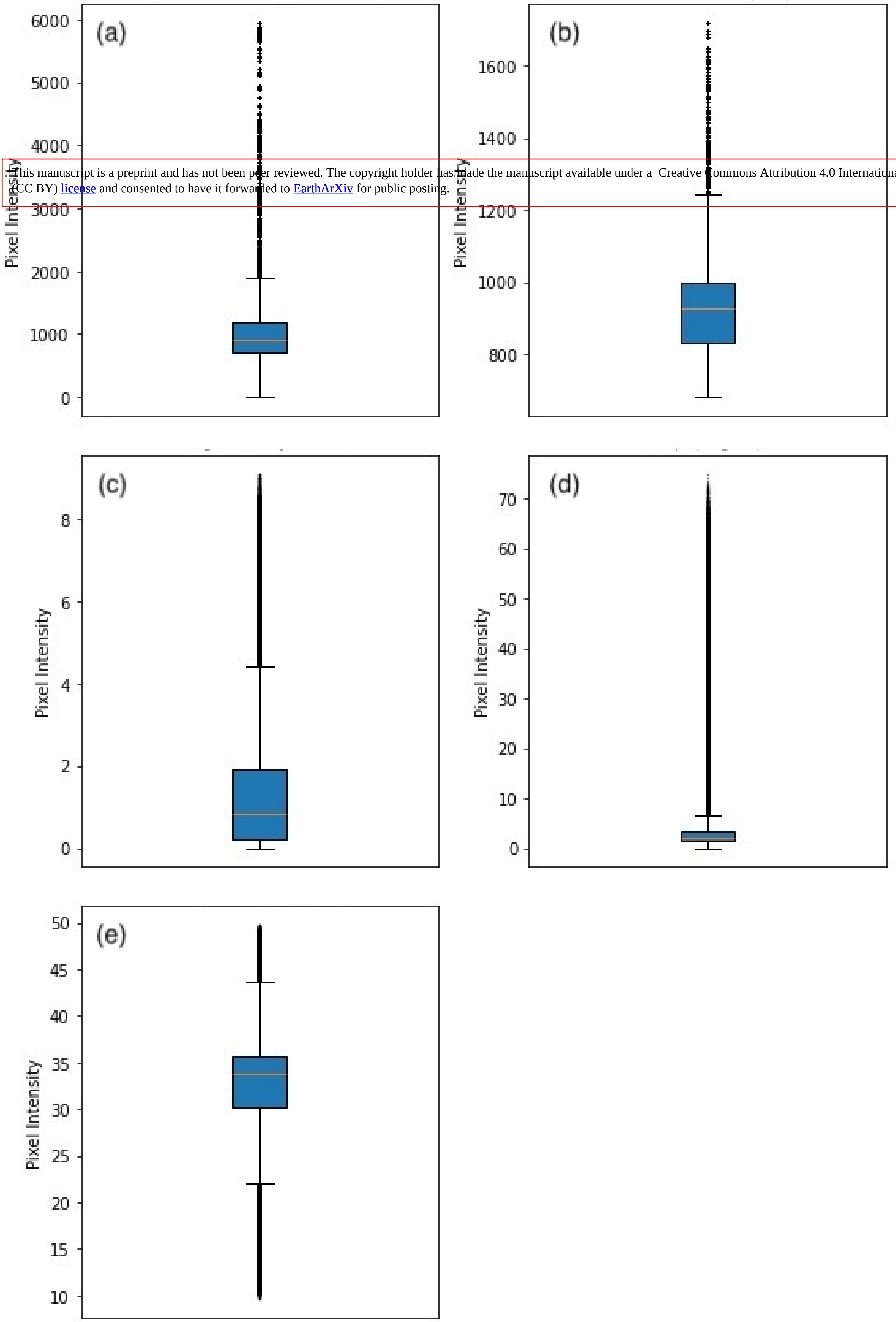
(a)
(b)
(c)
(d)
(e)
Pixel Intensity
6000
5000
4000
3000
2000
1000
0
1600
1400
1200
1000
800
8
6
4
2
70
60
50
40
30
20
10
45
35
25
15

FigS1

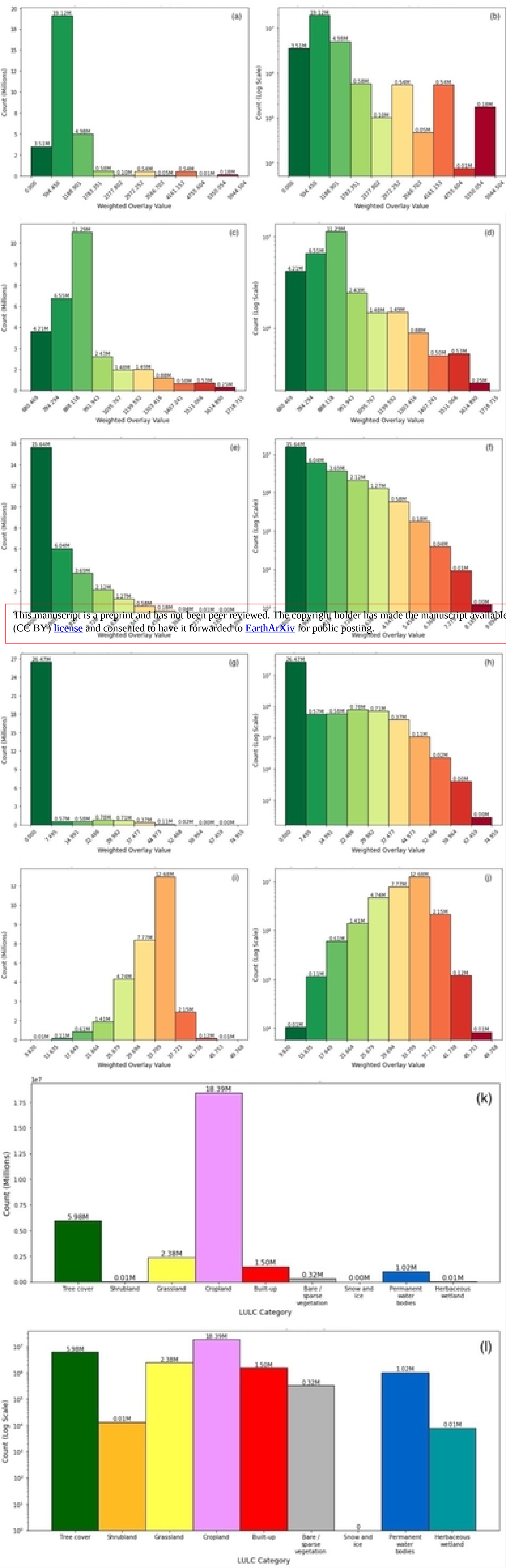
(a)
(b)
(c)
(d)
(e)
(f)
(g)
(h)
(i)
(j)
(k)
(l)
Weighted Overlay Value
Count (Millions)
Count (Log Scale)
LULC Category
Tree cover
Shrubland
Grassland
Cropland
Built-up
Bare / sparse vegetation
Snow and ice
Permanent water bodies
Herbaceous wetland
5.98M
0.01M
2.38M
18.39M
1.50M
0.32M
0.00M
1.02M
0.01M

FigS2

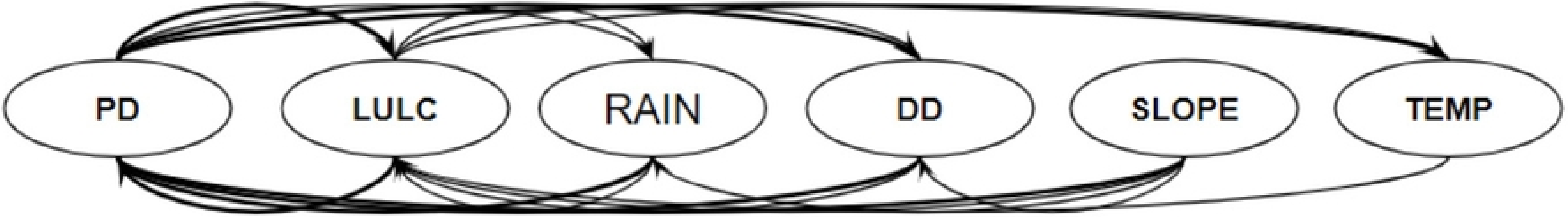

FigS3

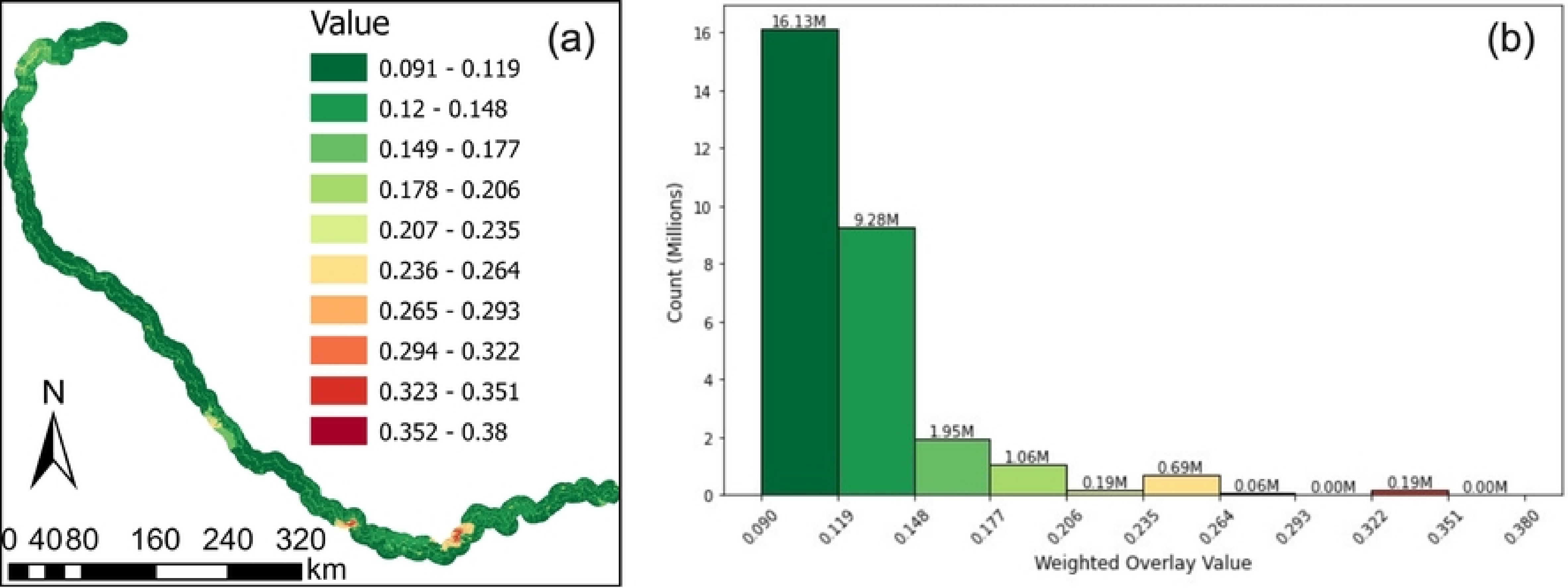
Value
(a)
0.091 - 0.119
0.12 - 0.148
0.149 - 0.177
0.178 - 0.206
0.207 - 0.235
0.236 - 0.264
0.265 - 0.293
0.294 - 0.322
0.323 - 0.351
0.352 - 0.38
N
0 40 80 160 240 320
km
(b)
16.13M
9.28M
1.95M
1.06M
0.19M
0.69M
0.06M
0.00M
0.19M
0.00M
Count (Millions)
0
2
4
6
8
10
12
14
16
0.090
0.119
0.148
0.177
0.206
0.235
0.264
0.293
0.322
0.351
0.380
Weighted Overlay Value

FigS4

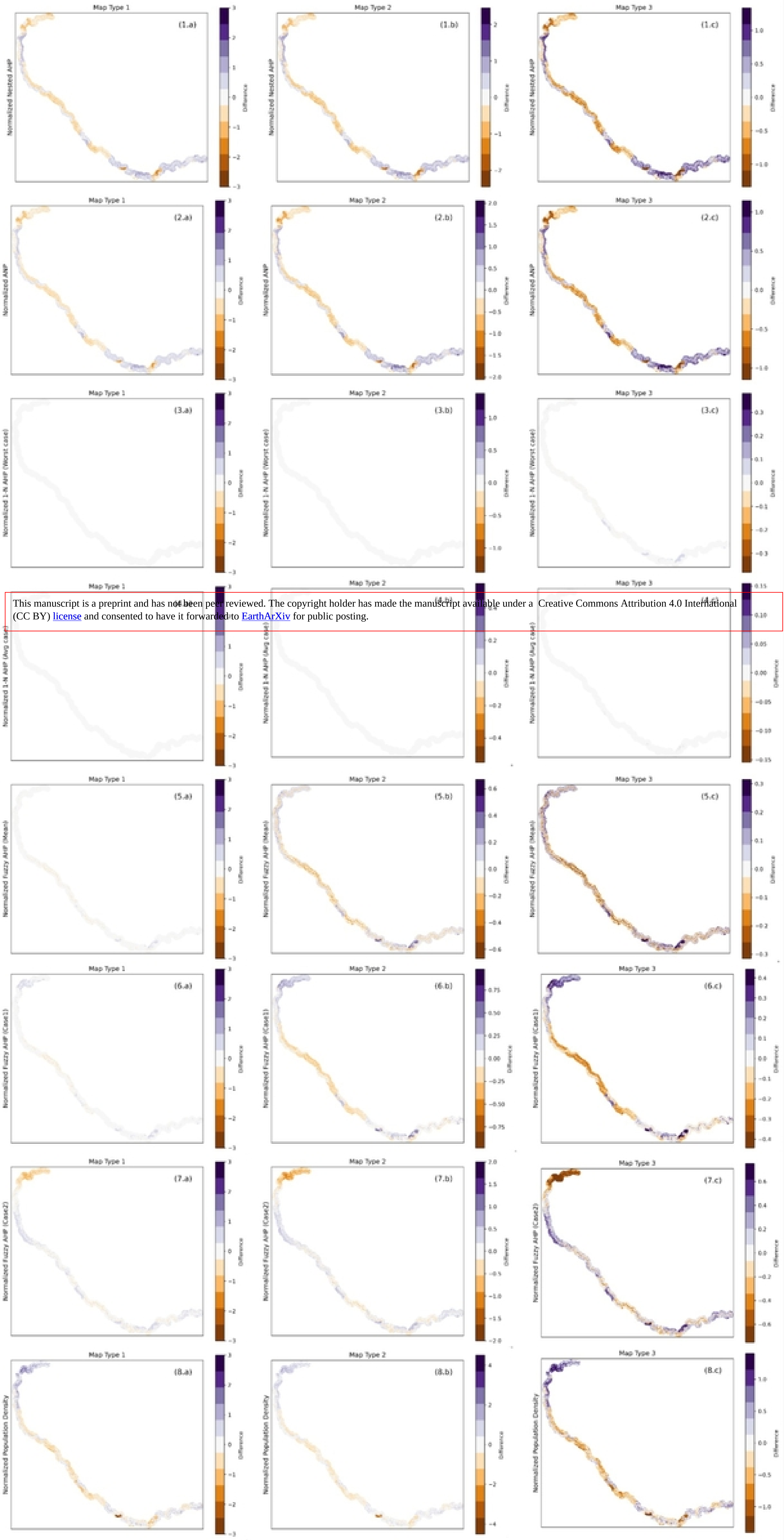

FigS5